Title: The Marine Isotope Stage 19 in the mid-latitude North Atlantic Ocean: astronomical signature and intra-interglacial variability

Corresponding Author: Dr. Patrizia Ferretti, PhD

Corresponding Author's Institution: Consiglio Nazionale delle Ricerche (CNR)

First Author: Patrizia Ferretti, PhD

Order of Authors: Patrizia Ferretti, PhD ; Simon Crowhurst; David Naafs; Carlo Barbante

Abstract: Since the seminal work by Hays, Imbrie and Shackleton (1976), a plethora of studies has demonstrated a correlation between orbital variations and climatic change. However, information on how changes in orbital boundary conditions affected the frequency and amplitude of millennial-scale climate variability is still fragmentary. The Marine Isotope Stage (MIS) 19, an interglacial centred at around 785 ka, provides an opportunity to pursue this question and test the hypothesis that the long-term processes set up the boundary conditions within which the short-term processes operate. Similarly to the current interglacial, MIS 19 is characterised by a minimum of the 400-kyr eccentricity cycle, subdued amplitude of precessional changes, and small amplitude variations in insolation. Here we examine the record of climatic conditions during MIS 19 using high-resolution stable isotope records from benthic and planktonic foraminifera from a sedimentary sequence in the North Atlantic (Integrated Ocean Drilling Program Expedition 306, Site U1313) in order to assess the stability and duration of this interglacial, and evaluate the climate system's response in the millennial band to known orbitally induced insolation changes. Benthic and planktonic foraminiferal $\delta 18O$ values indicate relatively stable conditions during the peak warmth of MIS 19, but sea-surface and deep-water reconstructions start diverging during the transition towards the glacial MIS 18, when large, cold excursions disrupt the surface waters whereas low amplitude millennial scale fluctuations persist in the deep waters as recorded by the oxygen isotope signal. The glacial inception occurred at ~779 ka, in agreement with an increased abundance of tetra-unsaturated alkenones, reflecting the influence of icebergs and associated meltwater pulses and high-latitude waters at the study site. After having combined the new results with previous data from the same site, and using a variety of time series analysis techniques, we evaluate the evolution of millennial climate variability in response to changing orbital boundary conditions during the early-middle Pleistocene. Suborbital variability in both surface- and deep-water records is mainly concentrated at a period of ~11 kyr and, additionally, at ~5.8 and ~3.9 kyr in the deep ocean; these periods are equal to harmonics of precession band oscillations. The fact that the response at the 11 kyr period increased over the same interval during which the amplitude of the response to the precessional cycle increased supports the notion that most of the variance in the 11 kyr band in the sedimentary record is nonlinearly transferred from precession band oscillations. Considering that these periodicities are important features in the equatorial and intertropical insolation, these observations are in line with the view that the low-latitude regions play an important role in the response of the climate system to the astronomical forcing. We conclude that

the effect of the orbitally induced insolation is of fundamental importance in regulating the timing and amplitude of millennial scale climate variability.

Highlights

- Harmonics of precession imprint in the North Atlantic (~11, 5.8 and 3.9 kyr cycles)
- Orbitally induced insolation is a plausible driver for millennial scale variability
- Cross-correlation coefficients confirm MIS 19 is a good analogue for the Holocene
- The glacial inception during Marine Isotope sub-Stage 19c is at ~779 ka
- From ~776 ka multiple events of iceberg discharges and ocean circulation disruption

1   **The Marine Isotope Stage 19 in the mid-latitude North Atlantic Ocean:**
2   **astronomical signature and intra-interglacial variability**
3
4
5   Patrizia Ferretti [a] *, Simon J. Crowhurst [b], B. David A. Naafs [c], Carlo Barbante [a, d]
6
7
8   [a] Consiglio Nazionale delle Ricerche, Istituto per la Dinamica dei Processi Ambientali
9   (CNR-IDPA), Calle Larga Santa Marta 2137, Venice I-30123, Italy
10
11   [b] The Godwin Laboratory for Palaeoclimate Research, Department of Earth Sciences,
12   University of Cambridge, Downing Street, Cambridge CB2 3EQ, United Kingdom
13
14   [c] Organic Geochemistry Unit, School of Chemistry and Cabot Institute, University of
15   Bristol, Cantock's Close, BS8 1TS Bristol, United Kingdom.
16
17   [d] Dipartimento di Scienze Ambientali, Informatica e Statistica, Università di Venezia
18   Calle Larga S. Marta 2137, Venice I-30123, Italy.
19
20   * Corresponding author.
21   Consiglio Nazionale delle Ricerche, Istituto per la Dinamica dei Processi Ambientali
22   (CNR-IDPA), Calle Larga Santa Marta 2137, Venice I-30123, Italy.
23   Tel.: +39 041 2348504; fax: +39 041 2348549.
24   E-mail address: patrizia.ferretti@idpa.cnr.it, patrizia.ferretti@unive.it (P. Ferretti).

1 **Abstract**

2 Since the seminal work by Hays, Imbrie and Shackleton (1976), a plethora of studies

3 has demonstrated a correlation between orbital variations and climatic change.

4 However, information on how changes in orbital boundary conditions affected the

5 frequency and amplitude of millennial-scale climate variability is still fragmentary.

6 The Marine Isotope Stage (MIS) 19, an interglacial centred at around 785 ka, provides

7 an opportunity to pursue this question and test the hypothesis that the long-term

8 processes set up the boundary conditions within which the short-term processes

9 operate. Similarly to the current interglacial, MIS 19 is characterised by a minimum

10 of the 400-kyr eccentricity cycle, subdued amplitude of precessional changes, and

11 small amplitude variations in insolation. Here we examine the record of climatic

12 conditions during MIS 19 using high-resolution stable isotope records from benthic

13 and planktonic foraminifera from a sedimentary sequence in the North Atlantic

14 (Integrated Ocean Drilling Program Expedition 306, Site U1313) in order to assess

15 the stability and duration of this interglacial, and evaluate the climate system's

16 response in the millennial band to known orbitally induced insolation changes.

17 Benthic and planktonic foraminiferal $\delta^{18}O$ values indicate relatively stable conditions

18 during the peak warmth of MIS 19, but sea-surface and deep-water reconstructions

19 start diverging during the transition towards the glacial MIS 18, when large, cold

20 excursions disrupt the surface waters whereas low amplitude millennial scale

21 fluctuations persist in the deep waters as recorded by the oxygen isotope signal. The

22 glacial inception occurred at ~779 ka, in agreement with an increased abundance of

23 tetra-unsaturated alkenones, reflecting the influence of icebergs and associated

24 meltwater pulses and high-latitude waters at the study site. After having combined the

25 new results with previous data from the same site, and using a variety of time series

1   analysis techniques, we evaluate the evolution of millennial climate variability in

2   response to changing orbital boundary conditions during the early-middle Pleistocene.

3   Suborbital variability in both surface- and deep-water records is mainly concentrated

4   at a period of ~11 kyr and, additionally, at ~5.8 and ~3.9 kyr in the deep ocean; these

5   periods are equal to harmonics of precession band oscillations. The fact that the

6   response at the 11 kyr period increased over the same interval during which the

7   amplitude of the response to the precessional cycle increased supports the notion that

8   most of the variance in the 11 kyr band in the sedimentary record is nonlinearly

9   transferred from precession band oscillations. Considering that these periodicities are

10   important features in the equatorial and intertropical insolation, these observations are

11   in line with the view that the low-latitude regions play an important role in the

12   response of the climate system to the astronomical forcing. We conclude that the

13   effect of the orbitally induced insolation is of fundamental importance in regulating

14   the timing and amplitude of millennial scale climate variability.

15

1. Introduction

It has long been recognised that the long-term climatic variations deduced from the geological records are driven by the insolation changes forced by variations in Earth orbital geometry (Adhémar, 1842; Berger, 1988; Croll, 1867, 1867; Hays et al., 1976). Whether these orbitally induced insolation changes modulated or even triggered climate variability in the millennial band is still open to question. A possible feature, which has hindered the inclusion of the orbital or astronomical input as a plausible forcing for rapid climate variability, has been the difference between the primary Milankovitch periods (i.e. the shortest ~19 kyr) and the timing of abrupt climate changes (a few kyr). However, the climate system may behave as a highly nonlinear system and it is conceivable that forcing with frequencies much lower (e.g. a few kyr) than those of its own free oscillations (e.g. ~100, 41, 19-23 kyr) can influence its response.

The potential for suborbital climate variability arising as a nonlinear response to Milankovitch forcing was suggested by modeling studies (e.g., Ghil and Le Treut, 1981; Le Treut and Ghil, 1983; Rial and Yang, 2007; Short et al., 1991; Wigley, 1976) and lately observed in different palaeoclimatic spectra (Hagelberg et al., 1994; Ortiz et al., 1999; Wara et al., 2000). Oscillations at frequencies equal to precession harmonics (~11 kyr and 5.5 kyr) have been identified in different surface water records (Billups et al., 2011; Hernández-Almeida et al., 2012; McIntyre and Molfino, 1996; Niemitz and Billups, 2005; Weirauch et al., 2008) and recently we have presented evidence that not only surface- but also deep-water records vary on such timescales during the Early Pleistocene (Marine Isotope Stages (MIS) 23-20, ~910 - 790 ka) in the North Atlantic Ocean (Integrated Ocean Drilling Program - IODP-Expedition 306, Site U1313) (Ferretti et al., 2010). The specific mechanisms by which

4

1 these orbitally induced insolation changes produced the observed climate responses

2 are still poorly understood; however, a good correlation between our surface and

3 deep-water hydrography reconstructions and the tropical insolation forcing have

4 supported the hypothesis that the timing of abrupt climate changes, as well as the

5 amplitude of millennial scale oscillations, may be strongly influenced by insolation

6 variations at the low latitudes.

7   In order to investigate the temporal extent of these events, and verify whether the

8 harmonics of precession were a recurring feature of the Pleistocene climatic

9 variability, here we extend our observations at IODP Site U1313 to an interval of time

10 characterized by different orbital configurations and place special emphasis on MIS

11 19. Similarly to the Holocene, MIS 19 was close to the minimum in the *c.* 400 kyr

12 eccentricity envelope (i.e. the Earth's orbit was close to circular) thus minimizing the

13 effect of precession; this is because eccentricity modulates the climatic precession

14 parameter which controls most of the long-term variations of the daily insolation

15 received from the Sun (Berger et al., 1993). It follows that the major feature of the

16 insolation over this interval is the small amplitude of its variations. We set out with

17 the aim of investigating millennial-scale variability in North Atlantic sea surface- and

18 deep-water hydrography during MIS 19 and comparing such variations with those

19 from our earlier study focusing on the older portion of the record (MIS 23-20). Our

20 final objective is the assessment of the nonlinear coupling to climatic forcing recorded

21 in the geological record via changes in orbital precession. More specifically, our

22 working hypothesis is that if the insolation determines, in the end, the timing and

23 amplitude of rapid climate change, during MIS 19 we would expect a weaker spectral

24 power at periodicities associated with the harmonics of the precession band, together

25 with relatively low amplitude oscillations aligned with intervals of low precessional

1   forcing (i.e. periods of low eccentricity). We will see that this appears to be the case.

2

3   **2. Regional setting**

4   The sediments used for this study were recovered from Site U1313, a reoccupation

5   of Deep Sea Drilling Project (DSDP) Leg 94 Site 607, during Expedition 306 of the

6   Integrated Ocean Drilling Program (Expedition 306 Scientists, 2006; Stein et al.,

7   2006). This site is located in the North Atlantic on the upper middle western flank of

8   the Mid-Atlantic Ridge, ~400 km WNW of the Azores (41°00'N, 32°58'W) (Fig. 1).

9   At present, Site U1313 is predominantly influenced by the surface waters of the North

10   Atlantic Current (Fratantoni, 2001) and, at a water depth of 3426 m, is under the

11   influence of North Atlantic Deep Water (NADW). During glacial periods however,

12   the site became regularly influenced by high-latitude waters as evidenced by low

13   alkenone-based SSTs and appearance of ice-rafted debris (Naafs et al., 2011; 2013).

14   In addition, the more negative carbon isotope values observed during glacials over the

15   Pleistocene indicates that this location is sensitive to past changes in the relative

16   contribution of high δ^{13}C NADW and low δ^{13}C southern source waters and to changes

17   in the locations of these two water masses (Ferretti et al., 2010; Raymo et al., 2004;

18   Raymo et al., 1990; Voelker et al., 2010).

19

20   **3. Materials and methods**

21   *3.1 Stable Isotopes*

22   The composite section of Site U1313 was sampled at a constant 1-cm spacing

23   following the shipboard secondary splice between 35.94 and 38.39 meters composite

24   depth (mcd), corresponding to the interval MIS 19. The spliced stratigraphic section

25   was refined postcruise using shipboard magnetostratigraphy, lightness and magnetic

1 susceptibility measurements to provide more accurate correlation points, and the

2 sampled depth-series corresponds to 36.30 and 38.40 revised meters composite depth

3 (rmcd) (= amended meters composite depth - amcd - in Naafs et al. (2012)).

4   Sediment samples were processed following standard procedures that involve

5 disaggregating the samples in reverse osmosis (RO) water overnight on an orbital

6 shaker and washing them through a 63 μm sieve to isolate the sand size fraction.

7 Changes in surface and deep-water hydrography were inferred from variations in

8 stable isotopes on planktonic and benthic foraminifera, respectively. About 20

9 specimens of the planktonic foraminifera *Globigerina bulloides* were used for each

10 mass spectrometric analysis to provide ample carbon dioxide; specimens were

11 selected from the 315-355 μm size fraction to minimize noise arising from isotopic

12 changes during ontogeny. Between 5 and 10 specimens of *Cibicidoides wuellerstorfi*

13 were picked, mostly from the fraction >212 μm. After picking, specimens were lightly

14 crushed and cleaned ultrasonically with methanol for a few seconds to remove fine-

15 grained particles; excess liquid and residues were then removed with a pipette, and

16 samples were dried under a vacuum hood. All isotope measurements were made using

17 a ThermoFinnigan-MAT 252 isotope ratio mass spectrometer coupled with a Kiel II

18 carbonate preparation device at the Serveis Científico-Tècnics of the University of

19 Barcelona and are reported referenced to the Vienna Pee Dee Belemnite (VPDB)

20 standard using NBS-19 for calibration. Analytical precision was better than 0.08 for

21 $\delta^{18}O$ and 0.04 for $\delta^{13}C$. *Cibicidoides wuellerstorfi* $\delta^{18}O$ values were adjusted for

22 species-specific offsets relative to *Uvigerina* spp. (widely considered to precipitate its

23 calcite in oxygen isotopic equilibrium with respect to seawater) by adding +0.64 ‰

24 VPDB (Shackleton and Opdyke, 1973).

25   Several duplicate measurements at the same depth were performed on *G. bulloides*

1   between 37.15 rmcd and 38.29 rmcd; this procedure was adopted not because the

2   results of the initial measurements were suspected to be aberrant but rather to confirm

3   the observed pattern of higher amplitude oscillations in the planktonic $\delta^{18}O$ signal.

4   The replicate analyses did not deviate from the original measurements and the results

5   were then averaged.

6

7   *3.2 Age model*

8   We tried several strategies for developing a geological time scale based on the

9   cyclicity observed at Site U1313, and the best approach was to develop an age model

10   within the Lisiecki and Raymo (2005) stack framework and subsequently confirm the

11   resulting depth-to-time conversion by fine-tuning of the extracted precession

12   component of the climate signal to the precession parameter. In detail, an initial

13   chronology was derived by correlating the Site U1313 benthic $\delta^{18}O$ signal to the

14   stacked $\delta^{18}O$ record of Lisiecki and Raymo (2005) (from now onwards LR04)

15   because this proved an effective and well-documented target for the lower part of the

16   sequence (Ferretti et al., 2010). Above 37.70 rmcd (*c.* 766 ka on this preliminary time

17   scale) however, it was not a straightforward process to bring the climate variability

18   observed at Site U1313 into phase with the LR04 tuning target, mainly because the

19   benthic $\delta^{18}O$ signal shows little variability in the most recent part of the record and

20   this pattern-matching exercise become ambiguous (Fig. 2a); the relatively stable

21   conditions recorded at Site U1313 diverge from other deep-water reconstructions

22   from the North Atlantic, where three distinct oscillations in $\delta^{18}O$ benthic values were

23   recorded during the MIS19c-19b transition (Ferretti et al., 2005; Kleiven et al., 2011)

24   (Fig. S1). On the other hand, this is an interval over which the planktonic record from

25   Site U1313 departs markedly from the benthic one by showing higher amplitude

8

1   oscillations (Fig. 2b). We then used orbital parameters to fine-tune our records based

2   on the LR04 chronology. The first step we performed was to join the new results from

3   MIS 19 with the previously published foraminiferal stable isotope records from this

4   site (Ferretti et al., 2010), in order to obtain a sequence long enough for statistical

5   analyses. The second step was to identify in this sequence the imprint of a particular

6   component of the orbital forcing and in particular to assess the presence of the higher

7   frequency orbital parameter, the precession component. Spectral analysis of the entire

8   length of these records on the initial LR04 chronology shows that there is a

9   concentration of power at the precession band in all the isotope records reconstructed

10   from Site U1313, and this component is strongest in the planktonic δ^{18}O. The third

11   step was to refine our age model by matching a 20 kyr filter of the planktonic δ^{18}O to

12   the precession index, while maintaining the LR04 stack (which exhibits significant

13   coherency with insolation in both the obliquity and precession bands) as the main

14   tuning framework. At the outset, the planktonic δ^{18}O dataset was filtered in the

15   precessional frequency range in the time domain because this procedure assists in

16   aligning core segments containing a precessional signal alongside the other primary

17   Milankovitch frequencies. We proceeded on the assumption that the δ^{18}O record has

18   responded to forcing with the same time-constant throughout the interval under

19   discussion, a premise that has been adopted for generating different timescales in the

20   last decades (among others, Shackleton et al. (1990)). In order to quantify the time-

21   constant, we have determined the phase relationship between precession and the

22   planktonic δ^{18}O record from core MD 95-2042 on the Iberian margin off southern

23   Portugal (Shackleton et al., 2000). Cross-spectral analysis of planktonic δ^{18}O from

24   core MD 95-2042 and precession shows that the planktonic δ^{18}O lags the precession

25   parameter by 3.3 kyr, and the same value was used to define the phase of Site U1313

1 planktonic $\delta^{18}O$ relatively to precession. The pattern-matching exercise at Site U1313

2 is a relative straightforward process even at above 37.70 rmcd (*c.* 778 ka on this time

3 scale), the depth at which the benthic $\delta^{18}O$ signal becomes quite smooth, permitting

4 an unambiguous match with the target to be achieved (Fig. 3). In this manner, the

5 refinement of our record by means of orbital tuning has arguably provided a more

6 accurate time scale than could have been achieved by solely correlating the benthic

7 $\delta^{18}O$ to the LR04 stack. For the lower part of the section, from 832 ka (MIS 21 to 23),

8 we rely on the initial chronology developed by Ferretti et al. (2010) matching the

9 sequence to LR04 stack, since there is no basis for major modification of the proposed

10 age model (Fig. 3). Fig. 4 shows the planktonic and benthic data on a timescale

11 derived by matching to the LR04 record in a manner consistent with the filtering

12 experiment (see also Figs S2 and S3). Table 1 lists the control points that we have

13 used to construct the time-series in Fig. 4 and Fig. 3c illustrates the sedimentation rate

14 picture that emerges from the refined time scales developed in this study. We

15 conclude that our record spans the time interval from *c.* 740 to 910 ka. The mean

16 sedimentation rate for MIS 19 is *c.* 4.5 cm/kyr, and the sampling interval of 1-cm

17 results in an average temporal resolution of 250 years.

18   Time-series analysis was performed to test for statistically significant cycles,

19 coherence, and relative phase of proxy signals. Spectral and cross-spectral analysis

20 was conducted with the ARAND software package

21 (http://www.ncdc.noaa.gov/paleo/softlib/) (Howell et al., 2006), which uses the

22 standard methods of Jenkins and Watts (1968). Confirmatory analyses and bandpass

23 filtering were carried out using Analyseries (Paillard et al., 1996), and REDFIT

24 (Schulz and Mudelsee, 2002) was used to help examine the statistical significance of

25 particular peaks. In addition, wavelet analysis was conducted to assess temporal

1 changes in the periodicity and amplitude of the oxygen isotope variability using the

2 software SOWAS provided by Douglas Maraun (Maraun and Kurths, 2004; Maraun

3 et al., 2007). Confirmatory wavelet analyses were performed using the interactive

4 program provided by C. Torrence and G. Compo and available at URL:

5 http://paos.colorado.edu/research/wavelets/.

6

7 **4. Results**

8   The oxygen and carbon isotope data from MIS 19-23 are plotted against estimated

9 age in Fig. 4. In order to isolate the low frequency components of our proxy records,

10 we have smoothed the data with a Gaussian interpolation with a 15 kyr window

11 width, which has the effect of providing some smoothing as well as interpolation (Fig.

12 5). Taking the difference between the full data and the Gaussian interpolation

13 removes the variability shared by the two records - that is the longer periodicity

14 components - leaving a residual that reflects the millennial-scale variability in the

15 isotope signal. The result of subtracting the Gaussian interpolation from the observed

16 record is shown in Fig. 5. Time series analyses were performed on the residuals with

17 the object of establishing the dominant periodicities impressed on these records and to

18 show how their amplitude varied over time. Spectral analysis and wavelet analysis are

19 illustrated in Figs 6, S5, and 7 respectively, whereas Fig. S4 presents the results of the

20 REDFIT test aimed to assess the statistical significance of the spectral peaks.

21   Three features stands out from the overall procedure, which includes the

22 calculation of the Gaussian interpolation, the residuals, cross-spectral analysis and

23 wavelet analysis. First, it is visually clear that the amplitude of the high frequency

24 signal in the planktonic and benthic foraminiferal residuals is far smaller during MIS

25 19c (Fig. 5). On the other hand, the amplitude of the planktonic δ^{18}O residual is quite

1   low during most of MIS 19 but higher amplitude oscillations are present during the

2   MIS 19-18 transition, from *c.* 778 ka. To some extent, this feature is shared by the

3   benthic carbon signal, although its range of variability is lower than during the

4   previous interglacial MIS 21. Second, time series analysis reveals a significant

5   concentration of power at a period of about 11 kyr in the planktonic $\delta^{18}O$, benthic

6    $\delta^{18}O$ and benthic $\delta^{13}C$ residuals (Fig. 6). Cross-spectra of planktonic $\delta^{18}O$ vs. benthic

7    $\delta^{18}O$ records indicate high coherency above the 95% confidence level in the 11 kyr

8   band; the phase offset between the two parameters is about -35°, which at this

9   periodicity indicates that benthic $\delta^{18}O$ leads planktonic $\delta^{18}O$ by about 1080 years

10   (Fig. 6a). Again, there is high coherency between the benthic $\delta^{18}O$ and benthic $\delta^{13}C$ in

11   the 11 kyr band, with a lag of benthic $\delta^{13}C$ against benthic $\delta^{18}O$ of about 43°, which at

12   this band corresponds to *c.*1.3 kyr (Fig. 6b). Moreover, well-marked spectral peaks

13   can be observed in the benthic $\delta^{18}O$ residual at the ~5.8, 3.9 and 1.7 kyr periodicities

14   and at the period of ~3.7 kyr in the benthic $\delta^{13}C$ residual (Figs 6 and 4S). Third, the

15   wavelet analysis seems to indicate changes in activity in the millennial band over the

16   interval of time analysed in this study, with power being less concentrated at ~11 kyr

17   in the most recent part of the time series (after around 820 ka) (Fig. 7).

18

19   **5. Discussion**

20   *5.1 Validation and discussion on the proposed chronology*

21   *5.1.1.Comparison of the climate cycles in the depth and time domains*

22   A quantitative understanding of millennial-scale climate variability beyond the last

23   climate cycle has been hindered by the critical role of age control in interpreting

24   millennial-scale changes and the difficulty of confidently placing the marine records

25   on an accurate time scale beyond the range of radiocarbon dating and the Greenland

1   ice core record. At Site U1313, we have attempted to present the MIS 19 data on a

2   time scale constrained using a specific approach reflecting the distinctive precession

3   signal at this site. Once the whole sequence had been put on a preliminary age model

4   based on the LR04 stack, and it had become clear that it displayed a 20 kyr cyclicity

5   on this time scale, it was possible to refine the age model using the precessional

6   component of the orbital forcing curve, while maintaining the LR04 stack as the main

7   tuning basis. It must be emphasized that this procedure that matches the sedimentary

8   cycles with a sequence of precession cycles does have the effect of enhancing the

9   coherence with precession. However, it should also be emphasized that this procedure

10   neither introduces the imprint of the precession signal in the sedimentary sequence

11   nor has any effect on the amplitude of the Milankovitch-scale climate cycles observed

12   at Site U1313. Indeed, after removing the longer periods dominating the records in the

13   depth domain, spectral analysis of the $\delta^{18}O$ data in the depth domain reveals

14   significant concentrations of spectral power at around 0.84 m and 0.52 m in the

15   benthic and planktonic oxygen isotope records (Fig. 8). When converted to time by

16   means of an average sedimentation rate at Site U1313 of ~4.3 cm/kyr, these well-

17   marked spectral peaks correspond to periodicities of ~19.5 kyr and ~12 kyr

18   respectively, and are consistent with a derivation from precession band variations. It

19   might be objected that the 12 kyr periodicity is too long to be a consistent harmonic of

20   the 19.5 kyr period. However, it must be also pointed out that, in order to make this

21   calculation, we proceed with the simplest assumption that the sedimentation rates

22   were constant throughout the interval considered in this study. This is obviously

23   implausible from the geological point of view, and Fig. 3c confirms that that the

24   sedimentation rate picture inferred at Site U1313 is much more complex than being

25   simply constant. Considering how vulnerable the climate cycles are to the distorting

1   non-sinusoidal effects of both the climate system and the geological archive (e.g. high

2   frequency changes in accumulation rate), the similarity between the expected

3   harmonic (11 kyr, Fig. 6) and the observed harmonic (12 kyr, Fig. 8) is striking. This

4   observation confirms that precession was significant and detectable in the sedimentary

5   sequence before the age model was developed and subsequently refined through the

6   precession signal, and we conclude that the interpretation of these periodicities is not

7   dependent on the choice of our particular age model. As we will discuss extensively

8   in section 5.2, the modulation of the 10-kyr filtered planktonic data and the

9   eccentricity modulation of the precession component in the model output are

10   remarkably similar and there seems little possibility that this match could have been

11   obtained with an incorrect time scale (Figs 10a and 10c). It would of course (as with

12   almost any varying time series) have been possible to introduce a distorted

13   precession-like signal by introducing uncontrolled and spurious accumulation rate

14   variations. The numerous chronological constraints surrounding any actual geological

15   time series from this geological interval, including accumulation rate constraints,

16   make it much more difficult to generate large-scale errors on these timescales than is

17   sometimes supposed (e.g. Proistosescu et al., 2012).

18

19   *5.1.2 The glacial inception during Marine Isotope sub-Stage 19c*

20   Another line of evidence supporting our age model interpretation is related to the

21   duration of interglacial conditions during MIS 19. The timing of the glacial inception

22   during MIS19 has been recently estimated to be *c.* 777.5 ka at Ocean Drilling

23   Program (ODP) Site 983 on the Gardar Drift in the North Atlantic and constrained by

24   the onset of the bipolar seesaw climate variability, which requires ice-sheets large

25   enough to produce iceberg discharges (Tzedakis et al., 2012). The onset of these

1   climatic changes on the Gardar Drift converges with an increased abundance of tetra-

2   unsaturated alkenones ($C_{37:4}$) at *c.* 779 ka at IODP Site U1313 (Fig. 9a), reflecting the

3   influence of icebergs and associated meltwater pulses together with high-latitude

4   waters at the study site (Naafs et al., 2011; Naafs et al., 2013). Sea-surface

5   temperature (SST) declines, as inferred by both the alkenones-based SSTs (Fig. 9b)

6   (Naafs et al., 2011) and the planktonic $\delta^{18}O$, are coeval with the arrival of polar melt

7   water to our core location reflecting iceberg discharges from circum-Atlantic ice

8   sheets (Naafs et al., 2011; 2013) and suggest that ice-sheets at that time reached

9   sufficient size to extend to North Atlantic coasts and calve along coastlines despite the

10   weak eccentricity-precession parameters and the subdued insolation forcing. Our

11   estimate for the timing of the glacial inception during MIS 19, constrained by an

12   increase in the relative proportion of tetraunsaturated C_{37} alkenone, is within the

13   uncertainties of the Gardar Drift age model, regardless of the two different dating

14   approaches, and provides a validation of our tuned timescale.

15   Increases in this compound also occurred from *c.* 776 ka onwards, suggesting

16   multiple events of enhanced iceberg discharges into the North Atlantic as a result of

17   instability of Northern Hemisphere ice sheets; the meltwater originating from these

18   icebergs decreased both sea surface temperature and salinity, and this is consistent

19   with the observed increased amplitude oscillations in the planktonic $\delta^{18}O$ signal that

20   disrupted the transition toward glacial MIS 18. Salinity perturbations, resulting from

21   iceberg discharges could have also reduced the meridional overturning circulation in

22   the Atlantic Ocean and affected millennial-scale fluctuations in deep water circulation

23   as recorded by pronounced millennial scale-variations in the benthic foraminiferal

24     $\delta^{13}C$ record (Fig. 9c).

25

1   *5.2 Harmonics of precession-induced oscillations*

2   The important conclusion that can be drawn from the examination of our isotope

3   records is that palaeoclimate spectra from Site U1313 clearly reveal a significant

4   concentration of power at a period of about 11 kyr; a well marked concentration of

5   variance is also present in the 5.8 kyr band in the benthic $\delta^{18}O$ record, and these

6   periodicities are very close to periods related to the second and fourth harmonics

7   predicted from the primary precessional components (Berger et al., 2006). While the

8   Milankovitch theory - that the timing of variations in global climate is paced by

9   variations in Earth's orbital parameters - has been incorporated in mainstream

10 literature, much less is known about high frequency variability resulting from a

11 transfer of variance from primary orbital frequencies.

12   The potential for a nonlinear climate response to Milankovitch forcing in the

13 millennial band has been predicted in modeling studies since the late 1970s (e.g.,

14 (Berger et al., 2006; Ghil and Le Treut, 1981; Le Treut and Ghil, 1983; Short et al.,

15 1991; Wigley, 1976). More recently, Rial and Yang (2007) illustrated an example of

16 such a mechanism by showing that there is an important effect of insolation on the

17 Dansgaard-Oeschger pulses of the last 100 ka recorded in the Greenland Ice Core

18 Project (GRIP) ice core, which these authors consider affects the timing of the abrupt

19 climate change episodes through a process related to frequency modulation. In more

20 detail, the high-pass filtered GRIP time series has been shown to have a power

21 spectrum with a main peak at 4.46 kyr and four flanking peaks at 2.97, 3.6, 6.2, and

22 9.3 kyr, which are consistent with the predicted line spectrum of a sinusoid of period

23 4.46 kyr frequency modulated by a 19 kyr oscillation. In order to make these

24 observations more concrete, these authors also demonstrated that the GRIP time series

25 could be closely reproduced by a simple, non-linear differential equation representing

1   the climate response forced by the Milankovitch-cycle determined insolation.

2   Although their conclusion, that the timing of abrupt climate changes may be strongly

3   influenced by insolation through frequency modulation, was based upon analyses of

4   the stable isotopes in the GRIP time series covering the last 100 ka, it is reasonable to

5   expect that the physical mechanisms involved and nature of the nonlinearities may

6   have been much the same when the orbital boundary conditions were different from

7   the last ice age, as for example in the early-middle Pleistocene.

8   The existence of a nonlinear climate system response to the Milankovitch band

9   processes has additionally been identified in other palaeoclimate data analyses, and

10   suborbital scale oscillations containing periodicities close to the second and fourth

11   harmonics of precession (*c.* 11 and 5.5 kyr respectively) have been observed in

12   surface records from different locations (Billups et al., 2011; Billups and Scheinwald,

13   2014; Hernández-Almeida et al., 2012; McIntyre and Molfino, 1996; Niemitz and

14   Billups, 2005; Weirauch et al., 2008). More recently, it has been shown that not only

15   surface- but also deep-water reconstructions from the North Atlantic contain the same

16   periodicities during the Middle Pleistocene (Billups et al., 2011; Ferretti et al., 2010),

17   suggesting that this nonlinear coupling to climatic forcing via changes in orbital

18   precession also affects the deep limb of the meridional overturning cell.

19   In this paper we show an additional reason to believe that changes in the Earth's

20   orbital geometry and their effect on the seasonal distribution of insolation are a

21   plausible driver for climate variability on millennial timescales at Site U1313.

22   Wavelet analyses of the $\delta^{18}O$ residuals, which yield information on both the

23   amplitude of periodic signals within the series and how this amplitude varies with

24   time, show significant concentration of variance close to half precession during the

25   portion of the record when precession forcing is also strong (880-830 ka) (Fig. 7).

1   Between 880 and 850 ka, when precession exhibits the largest amplitude variations of

2   the time interval considered in this study, spectral power in the benthic $\delta^{18}O$ record

3   also contains periodicities related to the fifth harmonic of precession (*c.* 3.9 kyr). On

4   the other hand, in the planktonic $\delta^{18}O$ record, lower - although still significant - power

5   in the 11 kyr band is displayed between 800-750 ka, which corresponds to an interval

6   of subdued precessional variations as a result of low eccentricity values. Considering

7   that the effect of precession on the seasonal distribution of solar radiation is also

8   modulated by orbital eccentricity, the major feature of the insolation over this time

9   intervals is the small amplitude of its variations. Thus, our results suggest a

10   dependence of climate variability on millennial timescales at Site U1313 to orbitally

11   induced insolation changes in such a way that insolation seems to drive or pace

12   climate change directly and proportionally during the interval of time considered in

13   this study.

14   In order to make these statements more concrete, we have reviewed the specific

15   mechanisms by which insolation changes produce the observed climate responses. A

16   possible scenario involves the generation of half precessional climate variability in the

17   Equatorial and intertropical regions, which is then advected to the high latitudes by

18   either atmospheric or oceanic circulation with little lag. In this scenario, a complex

19   response of maximum surface temperature to insolation forcing in equatorial regions

20   is generated when the perihelion of the Earth's orbit coincides with the vernal or

21   autumnal equinox; because this combination occurs twice in every precession cycle, it

22   creates a precession cycle harmonic at 10-12 cycle/kyr (Short et al., 1991). A direct

23   consequence of this process would be an amplified response of tropical precipitation

24   and temperature to changes in maximum summer insolation, a response that may then

25   be transferred from equatorial latitudes to the higher latitudes of the North Atlantic

1   via advective transport (Hagelberg et al., 1994; Short et al., 1991). Another scenario

2   that has been proposed to explain semiprecession cycles, that are phase coupled to

3   both precession and eccentricity, invokes the export of a Southern Hemisphere

4   precessional signal to the Northern Hemisphere; because the hemispheres are 180° out

5   of phase with respect to precession, this process generates semiprecession cycles in

6   the Northern Hemisphere (Rutherford and D'Hondt, 2000). Both the first and the

7   second scenario involve two precessional cycles that are 180° out of phase, but in the

8   first hypothesis the cycles are generated by the alignment of perihelion with each

9   equinox, while in the second one they are produced by the alignment of perihelion

10   with each solstice.

11   We have already demonstrated using cross-correlation coefficients that the first

12   scenario, which invokes a low-latitude equinoctial forcing, provides a more complete

13   and effective explanation for the observed proxy response at IODP Site U1313 during

14   MIS 23-20 than the high-latitude forcing (Ferretti et al., 2010). To evaluate if this is a

15   consistent feature of middle Pleistocene suborbital climate, we have extended to MIS

16   19 the comparison between our records and a) the insolation at the Equator in March–

17   April and September-October (Laskar et al., 2004) (Fig. 10b), in order to test the

18   hypothesis suggested by Short et al. (1991), and b) the insolation at both 65°N in

19   June-July and 65°S in December-January (Laskar et al., 2004) (Fig. 10d) to assess the

20   mechanism proposed by Rutherford and D'Hondt (2000). Figure 10 draws attention to

21   the overall similarity between trends in forcing and data and it is visually clear that a

22   very good match exists between the amplitude modulation in the 10-kyr Gaussian

23   bandpass filter of the planktonic and benthic foraminiferal $\delta^{18}O$ residual (Fig. 10c)

24   and insolation at the Equator during the Equinoxes (Fig. 10b). Our proxy records

25   mimics the equatorial insolation sequence remarkably well, both in terms of timing,

1   phase and amplitude. The attenuated signal in the benthic and planktonic isotope

2   records from *c.* 820 to 750 ka mirrors the subdued insolation variations and low

3   amplitude precessional changes (Fig. 10a), which are due to the modulation effect of

4   the 400-kyr eccentricity cycle. The phase offset between the timing of changes in the

5   insolation and the proxy records likely reflects a delay in the response of the climate

6   system to the astronomical forcing and, at least for the most recent part of the record

7   (*c.* 816-741 ka) is a consequence of the way in which the orbitally tuned age model

8   was reconstructed.

9

10   *5.3 MIS 19, an excellent analogue for the Holocene: insights from cross-correlation*

11   *coefficients between the forcing and the proxy response*

12   To investigate the match between the hypothesised possible forcings for the 10 kyr

13   cyclicity in U1313 - Equinoxes at the Equator and Solstices at both 65°N and 65°S -

14   we compared the amplitude modulation of the forcing and the proxy response, that we

15   extracted using the upper amplitude envelope of the variables. We ran a Pearson

16   Product-Moment cross-correlation at 1 kyr steps for the U1313 upper amplitude

17   envelope of the 10 kyr-filtered planktonic and benthic $\delta^{18}O$ response against the upper

18   amplitude envelope of possible 10 kyr forcings for a full 1.5 Ma interval of forcing

19   (Fig. 11). In our calculation of the cross-correlation coefficients, we focussed on the

20   upper amplitude envelopes of the variables only on the assumption that warming

21   responses would be driven by the higher insolation. This procedure at first sight might

22   appear pointless: why compare the climatic response to a wide range of orbital

23   forcings, most of which cannot possibly have been responsible for driving the

24   observed time series? However, the exercise addresses three questions: first, whether

25   the observed pattern of amplitude modulation is better explained by equinoctial or

1 solstice forcing, regardless of its precise placement in time by the tuning; second,

2 whether the amplitude modulation match is a coincidence, or is unlikely to have

3 arisen by chance in relation to the overall range of amplitude modulation over the last

4 1.5 Ma; and thirdly, whether the pattern of sub-Milankovitch amplitude modulation

5 observed around the geological interval MIS 19 is relevant to orbitally governed

6 climate behaviour at other intervals of the late Pleistocene, in particular the Holocene

7 and MIS 11, the latter of which is often considered as a potential analogue for the

8 Holocene and its future (Loutre and Berger, 2000, 2003).

9   The results appear to provide answers to all three questions (Fig. 11). The

10 calculated equinoctial forcing in the vicinity of MIS 19 is more strongly correlated

11 with the observed response than is the calculated solstice forcing (for benthic δ^{18}O, r^2

12 is a maximum 0.849 at 755 ka for the start of the sequence, versus 0.685 for solstice

13 forcing at 754 ka; for planktonic δ^{18}O, maximum r^2 for equinoctial forcing is 0.915 at

14 762 ka start age, versus a maximum 0.675 with 762 ka as the start of the sequence for

15 solstice forcing). The correlation between forcing and response is strong only in a few

16 intervals of the studied time range, and is therefore less likely to have arisen by

17 chance, especially considering that the 10 kyr cycles and their amplitudes were not

18 themselves tuned. In particular, the amplitude modulation of the 10 kyr cycle

19 observed in our data (and that we extracted using the upper amplitude envelope) from

20 *c.* 740-910 ka is consistent with forcing at only three places in the last 1.5 million

21 years: where it is (i.e. with the climate response occuring 750 kyr prior to the present),

22 380 ka ago, and close to the present. Therefore this comparison highlights the fact that

23 the orbital configuration apparently echoed by the climatic response is most closely

24 comparable to the configurations around MIS 11 and MIS 1, emphasising that the

25 millennial-scale variations around MIS 19 are particularly relevant to the Holocene. In

1   more general terms, the analysis presented here makes a very strong case for

2   concluding that during MIS 19 the orbital forcing at sub-Milankovitch periodicities -

3   and the climate response at this site - is very close to that which we might expect at

4   present and in the future (i.e. next 5 kyr) if natural rather than anthropogenic forcings

5   govern the climate behaviour.

6

7   *5.4 Phasing of harmonics of precession events*

8   The nature of the phase relationship among co-registered proxies from IODP Site

9   U1313 clearly deserves some attention. Cross-spectral analysis shows that benthic and

10   planktonic isotope variability is concentrated in the half-precession bandwidth, with

11   high coherency, and with the benthic $\delta^{18}O$ leading both planktonic $\delta^{18}O$ and benthic

12   $\delta^{13}C$ by around 1080 and 1300 years, respectively (Fig. 6). At DSDP Site 607, of

13   which Site U1313 represents a reoccupation, sea surface temperature lags behind

14   benthic $\delta^{18}O$ by around 3000 years in the precessional band, and benthic $\delta^{13}C$ also

15   shows a substantial lag behind $\delta^{18}O$ (Ruddiman et al., 1989); at this site, the phase

16   relationship is evaluated on a longer periodicity but, very interestingly, the same

17   sequence seems to apply, even if less quickly. Thus, palaeoclimate variability in the

18   precession band displays the same phasing as variability at periodicities equal to half-

19   precession harmonic, indicating that the same sequence of events characterised the

20   climate oscillations involved, at both primary and harmonic frequencies. One of the

21   difficulties of understanding such phase relationships is represented by the fact that

22   each climate proxy time series is influenced by different components of the climate

23   system and, in turn, each component has potentially a different phase relative to its

24   orbital forcing. In particular, the benthic $\delta^{18}O$ signal reflects a combination of deep-

25   water temperature effects and a water $\delta^{18}O$ component; in turn, the water $\delta^{18}O$ signal

1 echoes both global effects (i.e. ice volume) and local hydrographic effects due to

2 changes in the T - $\delta^{18}O$ signature of deep-water bathing the core site. The benthic

3 $\delta^{18}O$ signal has recently been deconvolved into its temperature and water $\delta^{18}O$

4 components at ODP Site 1123 in the Southwest Pacific (Elderfield et al., 2012;

5 Elderfield et al., 2010); however, the phasing inferred for the different components of

6 the benthic $\delta^{18}O$ in the SW Pacific signal does not necessarily apply to Site U1313.

7 This is because Site U1313 is more affected by changes in the relative contribution of

8 northern and southern-sourced water masses than Site 1123, and because of the long

9 oceanic transit time of the water $\delta^{18}O$ from the North Atlantic to the deep SW Pacific

10 (Skinner et al., 2003). We speculate that the phase relationship between the planktonic

11 and benthic $\delta^{18}O$ may indicate that the benthic $\delta^{18}O$ is responding more immediately

12 to the forcing than the surface $\delta^{18}O$. If the $\delta^{18}O$ variations reflect temperature

13 differences in the water masses (most likely), then this phase relationship suggests

14 that the temperature of deep-water in the Northern Atlantic Ocean changes somewhat

15 ahead of the surface water temperature, and therefore that such sub-Milankovitch

16 surface temperature changes in this part of the ocean are mainly initiated by changes

17 elsewhere in the global ocean surface, and transferred to this part of the North

18 Atlantic surface ocean by secondary processes such as changes in the position of the

19 polar front. Another hypothesis would be that changes in the $\delta^{18}O$ of the seawater

20 itself resulting from ice volume changes at sub-Milankovitch periodicities are

21 transferred to the North Atlantic surface only after a delay, but this seems harder to

22 envisage.

23 Another complex climate proxy is the benthic $\delta^{13}C$ signal, being affected by

24 multiple parameters (e.g. aging and mixing of water masses, temperature-dependent

25 air-sea exchange, organic carbon sequestered on the continents and continental

shelves, as well as long-term changes in the isotopic composition of rivers). Also in

this specific case, each parameter has the potential to show a different phase relative

to orbital forcing. Evidence of coupling between sea surface processes and deep water

circulation may be inferred from concurrent shifts in the benthic $\delta^{13}C$ and planktonic

$\delta^{18}O$ values. This is because, in the modern ocean, formation of NADW is contingent

upon the temperature and salinity of the surface waters, and the extent to which these

waters are cooled in winter at high latitudes; past changes in the North Atlantic

surface circulation, having an influence on these parameters, could also have modified

the rate of NADW production. Variability in the 11 kyr band has been inferred in both

the benthic $\delta^{13}C$ and planktonic $\delta^{18}O$ at Site U1313; however, no coherency is present

despite the spectral peak in the half precession bandwidth (Fig. S5). This means that

the lack of significant coherency between the benthic $\delta^{13}C$ and planktonic $\delta^{18}O$

residuals preclude a meaningful evaluation of the phase evolution in the interval

analysed. Although these observations clearly indicate that surface- and deep-water

records contain sub-orbital scale variation in the same band, they fail to unequivocally

rule in a unique mechanism by which they were triggered.

5.5 The role of the insolation

The other important conclusion that can be drawn from the examination of the 11

kyr part of the variance in the several signals is that even during periods of low

eccentricity, low precession and low amplitude insolation variations, as occurred

during MIS 19, the insolation appears to remain a plausible driver for millennial scale

climate variability at Site U1313. Frequency analyses of different time series from

deep-sea sediment cores covering the last 1.5 Ma have recently suggested a complex

picture of the relationship between climate response and astronomical forcing, where

1 the entrained response of the climate system is intermittent, alternating intervals of

2 'capture' and 'escape' from the forcing (Clark et al., 2006). Although the system

3 seems to jump from one state to the other at unpredictable times when stimulated by

4 the low-frequency forcing, this process seems to be governed by predictable

5 background states. Nonlinearities can generate randomness, in the same way as a

6 nonlinear climate response forced by the Milankovitch insolation could have

7 determined the apparently random Dansgaard-Oescher cycles of the last 100 ka

8 (Braun et al., 2008; Rial and Yang, 2007). Our results do not preclude the possibility

9 of such a complex scenario. That is, we propose here that insolation drives or paces

10 rapid climate change directly and proportionally in the time slice analysed in this

11 study, and our reconstruction appears to represent a period during which the climate

12 system is 'captured' by the forcing. However, we are aware that these observations do

13 not rule out the possibility that this is only part of a more complex picture

14 characterised by an alternation of different states.

15

16 **6. Conclusions**

17   Reliable predictions of future global climate rely upon understanding its complex

18 history. MIS 19, during the mid-Pleistocene transition, is a period during which the

19 insolation appears comparable to the current orbital geometry: it is characterised by a

20 subdued amplitude of precession as a consequence of the modulating effect of the 400

21 kyr eccentricity cycle. The phasing between precession and obliquity is also very

22 similar during the Holocene and MIS 19, making this marine isotopic stage a potential

23 astronomical analogue for the Holocene and its future evolution if this remains

24 governed by natural forcing (Loutre and Berger, 2000). In order to investigate

25 whether the orbital insolation influenced climate variability in the millennial band and

1   whether there are interactions between orbital and suborbital components of climate

2   variability, we have reconstructed high-resolution records of surface- and deep-water

3   hydrography from the North Atlantic Ocean during MIS 19. In agreement with our

4   earlier study focusing on the older portion of the record (MIS 23-20), we propose that

5   climate variations at sub-Milankovitch frequencies are amplitude and frequency

6   modulated by the harmonics of the precession forcing. Benthic and planktonic stable

7   isotope records from IODP Site U1313 document lower amplitude oscillations during

8   MIS 19, as a result of the weak eccentricity-precession forcing; moreover, time series

9   analysis illustrates that these variations still have a significant – although weaker than

10 during MIS 23-20 - concentration of spectral power centered on periods of ~11 kyr, in

11 both surface and deep water records, and 5.8 kyr in the benthic oxygen signal. This

12 timing is close to peaks expected from the second and fourth harmonics of the

13 precessional component of the insolation forcing and we suggest that forcing from

14 low latitudes is implicated in the origin of the harmonics of precession cycles

15 observed at Site U1313. The precise mechanism by which the energy is transported

16 into high latitudes away from equatorial regions is not easy to reconstruct from

17 available proxy records, but experiments with Earth System models may provide

18 useful insights into the way the climatic signal is transferred in the North Atlantic. On

19 the other hand, although insolation seems to be the most plausible trigger for

20 millennial scale variability, its extent depends also on the overall state of the climate

21 system, as it occurred during the transition towards MIS 18 when large, cold

22 excursions disrupted the surface waters due to instability of the Northern Hemisphere

23 ice sheets.

24   In summary, our results suggest that the variables measured by proxies are

25 replicated in cycles apparently paced by orbital changes, suggesting the climate

1 system is to a significant extent understandable and deterministic, being contingent

2 upon both forcing and previous history. If other climate records from different time

3 intervals and locations confirm our conclusions - that is, the insolation determines, in

4 the end, the timing and amplitude of rapid climate change - these results will have

5 important implications in the context of future climate change. Cross-correlation

6 coefficients between forcing and our proxy records show that during MIS 19 the

7 orbital forcing at sub-Milankovitch periodicities, apparently echoed by the climatic

8 response, is very close to that which we might expect at present and in the near future.

9 This in turn implies the intriguing possibility that, as stated by Rial and Yang (2007),

10 "since the insolation is certainly predictable, when climate models become reliable

11 enough, abrupt climate change may also become predictable" to the extent that the

12 behaviour of the climate system operates within the framework of its behaviour earlier

13 in the recent geological record.

14
34
35 **Appendix A. Supplementary material**
36   Supplementary data associated with this article can be found, in the online version,
37 at doi:xxx.

References

Adhémar, J.A., 1842. Révolutions de la mer, Privately published, Paris.

Berger, A., 1988. Milankovitch theory and climate. Reviews of Geophysics 26, 624-657.

Berger, A., Loutre, M.-F., Tricot, C., 1993. Insolation and Earth's orbital periods. Journal of Geophysical Research: Atmospheres 98, 10341-10362.

Berger, A., Loutre, M.F., Melice, J.L., 2006. Equatorial insolation: from precession harmonics to eccentricity frequencies. Climate of the Past 2, 131-136.

Billups, K., Rabideaux, N., Stoffel, J., 2011. Suborbital-scale surface and deep water records in the subtropical North Atlantic: implications on thermohaline overturn. Quaternary Science Reviews 30, 2976-2987.

Billups, K., Scheinwald, A., 2014. Origin of millennial-scale climate signals in the subtropical North Atlantic. Paleoceanography 29, 612-627, doi:10.1002/2014PA002641.

Braun, H., Ditlevsen, P., Chialvo, D.R., 2008. Solar forced Dansgaard-Oeschger events and their phase relation with solar proxies. Geophysical Research Letters 35, L06703.

Clark, P.U., Archer, D., Pollard, D., Blum, J.D., Rial, J.A., Brovkin, V., Mix, A.C., Pisias, N.G., Roy, M., 2006. The middle Pleistocene transition: characteristics, mechanisms, and implications for long-term changes in atmospheric pCO_2. Quaternary Science Reviews 25, 3150-3184.

Croll, J., 1867. On the change in the obliquity of the ecliptic, its influence on the climate of the polar regions and on the level of the sea. Philosophical Magazine 33, 426-445.

Croll, J., 1867. On the eccentricity of the earth's orbit, and its physical relations to the glacial epoch. Philosophical Magazine 33, 119-131.

Elderfield, H., Ferretti, P., Greaves, M., Crowhurst, S., McCave, I.N., Hodell, D., Piotrowski, A.M., 2012. Evolution of Ocean Temperature and Ice Volume Through the Mid-Pleistocene Climate Transition. Science 337, 704-709.

Elderfield, H., M., G., Barker, S., Hall, I.R., Tripati, A., Ferretti, P., Crowhurst, S., Booth, L., Daunt, C., 2010. A record of bottom water temperature and seawater ™^{18}O for the Southern Ocean over the past 440 kyr based on Mg/Ca of benthic foraminiferal Uvigerina spp. Quaternary Science Reviews 29, 160-169.

Expedition 306 Scientists, 2006. Site U1313. In: Channell, J.E.T., Kanamatsu, T., Sato, T., Stein, R., Alvarez Zarikian, C.A., Malone, M.J., Expedition 303/306 Scientists, (Eds.), Proc. IODP, 306. Integrated Ocean Drilling Program Management International, Inc., College Station TX. doi:10.2204/iodp.proc.303306.303112.302006.

Ferretti, P., Crowhurst, S.J., Hall, M.A., Cacho, I., 2010. North Atlantic millennial-scale climate variability 910 to 790 ka and the role of the equatorial insolation forcing. Earth and Planetary Science Letters 293, 28-41, doi:10.1016/j.epsl.2010.1002.1016.

Ferretti, P., Shackleton, N.J., Rio, D., Hall, M.A., 2005. Early-Middle Pleistocene deep circulation in the western subtropical Atlantic: Southern Hemisphere modulation of the North Atlantic Ocean, in: Head, M.J., Gibbard, P.L., (Eds.), Early-Middle Pleistocene transitions: the land ocean evidence 247. The Geological Society, London, pp. 131-145.

Fratantoni, D.M., 2001. North Atlantic surface circulation during the 1990's observed with satellite-tracked drifters. Journal of Geophysical Research 106, 22067-22093.

Ghil, M., Le Treut, H., 1981. A climate model with cryodynamics and geodynamics. Journal of Geophysical Research: Oceans 86, 5262-5270.

Hagelberg, T., Bond, G., De Menocal, P., 1994. Milankovitch band focing of sub-milankovitch climate variability during the Pleistocene. Paleoceanography 9, 545-558.

Hays, J.D., Imbrie, J., Shackleton, N.J., 1976. Variations in the Earth's Orbit: Pacemaker of the Ice Ages. Science 194, 1121-1132.

Hernández-Almeida, I., Sierro, F.J., Cacho, I., Flores, J.A., 2012. Impact of suborbital climate changes in the North Atlantic on ice sheet dynamics at the Mid-Pleistocene Transition. Paleoceanography 27, PA3214.

Howell, P., Pisias, N.J., Ballance, J., Baughman, J., Ochs, L., ARAND Time-Series Analysis Software, Brown University, Providence RI. Available at http://www.ncdc.noaa.gov/paleo/softlib/arand/arand.html, 2006.

Jenkins, G.M., Watts, D.G., 1968. Spectral analysis and its applications, Holden-Day, San Francisco, 525 pp.

Kleiven, H.F., Hall, I.R., McCave, I.N., Knorr, G., Jansen, E., 2011. Coupled deep-water flow and climate variabiliy in the Middle Pleistocene North Atlantic. Geology 39, 343-346, doi: 310.1130/G31651.31651.

Laskar, J., Robutel, P., Joutel, F., Gastineau, M., Correia, A.C.M., Levrard, B., 2004. A long-term numerical solution for the insolation quantities of the Earth. Astronomy & Astrophysics 428, 261-285, DOI: 210.1051/0004-6361:20041335.

Le Treut, H., Ghil, M., 1983. Orbital forcing, climatic interactions, and glaciation cycles. Journal of Geophysical Research: Oceans 88, 5167-5190.

Lisiecki, L.E., Raymo, M.E., 2005. A Pliocene-Pleistocene stack of 57 globally distributed benthic $\delta^{18}O$ records. Paleoceanography 20, PA1003, doi:1010.1029/2004PA001071.

Loutre, M.F., Berger, A., 2000. Future Climatic Changes: Are We Entering an Exceptionally Long Interglacial? Climatic Change 46, 61-90, 10.1023/A:1005559827189.

Loutre, M.F., Berger, A., 2003. Marine Isotope Stage 11 as an analogue for the present interglacial. Global and Planetary Change 36, 209-217.

Maraun, D., Kurths, J., 2004. Cross wavelet analysis: significance testing and pitfalls. Nonlinear Processes in Geophysics 11, 505-514.

Maraun, D., Kurths, J., Holschneider, M., 2007. Nonstationary Gaussian processes in wavelet domain: Synthesis, estimation, and significance testing. Physical Review E 75, 016707.

McIntyre, A., Molfino, B., 1996. Forcing of Atlantic equatorial and subpolar millennial cycles by precession. Science 274, 1867-1870.

Naafs, B.D.A., Hefter, J., Acton, G., Haug, G.H., Martínez-Garcia, A., Pancost, R., Stein, R., 2012. Strengthening of North American dust sources during the late Pliocene (2.7 Ma). Earth and Planetary Science Letters 317-318, 8-19.

Naafs, B.D.A., Hefter, J., Ferretti, P., Stein, R., Haug, G.H., 2011. Sea surface temperatures did not control the first occurrence of Hudson Strait Heinrich Events during MIS 16. Paleoceanography 26, PA4201, 4210.1029/2011PA002135.

Naafs, B.D.A., Hefter, J., Stein, R., 2013. Millennial-scale ice rafting events and Hudson Strait Heinrich(-like) Events during the late Pliocene and Pleistocene: a review. Quaternary Science Reviews 80, 1-28.

Niemitz, M.D., Billups, K., 2005. Millennial-scale variability in western tropical Atlantic surface ocean hydrography during the early Pliocene. Marine Micropaleontology 54, 155-166.

Ortiz, J., Mix, A., Harris, S., O'Connell, S., 1999. Diffuse spectral reflectance as a proxy for percent carbonate content in North Atlantic sediments. Paleoceanography 14, 171-186.

Paillard, D.L., Labeyrie, L., Yiou, P., 1996. Macintosh program performs time-series analysis. Eos Transactions American Geophysical Union 77, 379.

Proistosescu, C., Huybers, P., Maloof, A.C., 2012. To tune or not to tune: Detecting orbital variability in Oligo-Miocene climate records. Earth and Planetary Science Letters 325-326, 100-107.

Raymo, M.E., Oppo, D.W., Flower, B.P., Hodell, D.A., McManus, J.F., Venz, K.A., Kleiven, K.F., McIntyre, K., 2004. Stability of North Atlantic water masses in face of pronounced climate variability during the Pleistocene. Paleoceanography 19, PA2008, doi:2010.1029/2003PA000921.

Raymo, M.E., Ruddiman, W.F., Shackleton, N.J., Oppo, D.W., 1990. Evolution of Atlantic-Pacific $\delta^{13}C$ gradients over the last 2.5 m.y. Earth and Planetary Science Letters 97, 353-368.

Rial, J.A., Yang, M., 2007. Is the frequency of abrupt climate change modulated by the orbital insolation? Ocean Circulation: Mechanisms and Impacts - Past and Future Changes of Meridional Overturning, Geophys. Monogr. Ser. 173. AGU, Washington, DC, pp. 167-174.

Ruddiman, W.F., Raymo, M.E., Martinson, D.G., Clement, B.M., Backman, J., 1989. Pleistocene evolution: Northern hemisphere ice sheets and North Atlantic Ocean. Paleoceanography 4, 353-412.

Rutherford, S., D'Hondt, S., 2000. Early onset and tropical forcing of 100,000-year Pleistocene glacial cycles. Nature 408, 72-75.

Schulz, M., Mudelsee, M., 2002. REDFIT: estimating red-noise spectra directly from Unevenly spaced paleoclimatic time series. Computers and Geosciences 28, 421-426.

Shackleton, N.J., Berger, A., Peltier, W.R., 1990. An alternative astronomical calibration of the lower Pleistocene timescale based on ODP Site 677. Transactions of the Royal Society of Edinburgh: Earth Sciences 81, 251-261.

Shackleton, N.J., Hall, M.A., Vincent, E., 2000. Phase relationships between millennial-scale events 64,000-24,000 years ago. Paleoceanography 15, 565-569.

Shackleton, N.J., Opdyke, N.D., 1973. Oxygen isotope and palaeomagnetic stratigraphy of equatorial Pacific core V28-238: oxygen isotope temperatures and ice volumes on a 10^5 year and 10^6 year scale. Journal of Quaternary Research 3, 39-55.

Short, D.A., Mengel, J.D., Crowley, T.J., Hyde, W.T., North, G.R., 1991. Filtering of Milankovitch Cycles by Earth's Geography. Quaternary Research 35, 157-173.

Skinner, L.C., Shackleton, N.J., Elderfield, H., 2003. Millennial-scale variability of deep-water temperature and $\delta^{18}O_{dw}$ indicating deep water source variations in the Northeast Atlantic, 0-34 cal. ka BP. Geochemistry Geophysics Geosystems 4, 1098, doi:1010.1029/2003GC000585.

1   Stein, R., Kanamatsu, T., Alvarez-Zarikian, C., Higgins, S.M., Channell, J.E.T.,
2   Aboud, E., Ohno, M., Acton, G.D., Akimoto, K., Bailey, I., Bjørklund, K.R.,
3   Evans, H., Nielsen, S.H.H., Fang, N., Ferretti, P., Gruetzner, J., Guyodo,
4   Y.J.B., Hagino, K., Harris, R., Hatakeda, K., Hefter, J., Judge, S.A., Kulbanek,
5   D.K., Nanayama, F., Rashid, H., Sierro Sanchez, F.J., Voelker, A., Zhai, Q.,
6   2006. North Atlantic paleoceanography: The last five million years. Eos,
7   Transactions American Geophysical Union 87, 129-133.
8   Tzedakis, P.C., Channell, J.E.T., Hodell, D.A., Kleiven, H.F., Skinner, L.C., 2012.
9   Determining the natural length of the current interglacial. Nature Geoscience
10   5, 138-141.
11 Voelker, A.H.L., Rodrigues, T., Billups, K., Oppo, D., McManus, J., Stein, R., Hefter,
12   J., Grimalt, J.O., 2010. Variations in mid-latitude North Atlantic surface water
13   properties during the mid-Brunhes (MIS 9–14) and their implications for the
14   thermohaline circulation. Climate of the Past 6, 531-552.
15 Wara, M.W., Ravelo, A.C., Revenaugh, J.S., 2000. The pacemaker always rings
16   twice. Paleoceanography 15, 616-624.
17 Weirauch, D., Billups, K., Martin, P., 2008. Evolution of millennial-scale climate
18   variability during the mid-Pleistocene. Paleoceanography 23, PA3216,
19   doi:3210.1029/2007PA001584.
20 Wigley, T.M.L., 1976. Spectral analysis and the astronomical theory of climatic
21   change. Nature 264, 629-631.
22
23

1 **Figure captions**

2 Figure 1: Location map for IODP Site U1313 (41°00'N, 32°58'W, 3426 m water

3 depth) together with other sites cited in this study: ODP Site 983 (60°23'N 23°38'W,

4 1985 m water depth), ODP Site 1063 (33°41'N 57°36'W, 4584 m water depth), IODP

5 Site U1308 (49°53'N 24°14'W, 3872 m water depth). Major surface water currents in

6 the North Atlantic are from Fratantoni (2001). GS = Gulf Stream; NAC = North

7 Atlantic Current

8

9 Figure 2: Preliminary chronology for IODP Site U1313 after tuning the benthic

10 oxygen isotope data for IODP Site U1313 to the Lisiecki and Raymo stack (2005). (a)

11 Benthic $\delta^{18}O$ record from the LR04 stack (Lisiecki and Raymo, 2005) (green line) and

12 from IODP Site U1313 (red line) on the LR04 stack time scale. Black dots identify

13 the age control points; (b) Planktonic $\delta^{18}O$ record from IODP Site U1313 on the LR04

14 stack time scale (blue line). From c. 766 ka, the benthic oxygen isotope record of Site

15 U1313 diverges from the LR04 stack by showing little variability in the most recent

16 part of the record, and the pattern-matching exercise becomes ambiguous.

17 Adjustments were made to take into account taxon-dependent departures from

18 isotopic equilibrium by adding 0.64‰ VPDB to *C. wuellerstorfi* $\delta^{18}O$ values

19 (Shackleton and Opdyke, 1973).

20

21 Figure 3: Final chronology for IODP Site U1313 after using the orbital parameters to

22 fine-tune our initial age model based on the Lisiecki and Raymo stack (2005) (Fig. 2).

23 Oxygen isotope record for planktonic foraminifera in Site U1313 (blue line in Fig.

24 3a), filtered in the time domain (orange line in Figs 3a and 3b), and compared with the

25 precession index (e*sin ω, where e = eccentricity and ω is the longitude of perihelion)

1   (Laskar et al., 2004) lagged by 3.3 kyr (violet line in Fig. 3b). The Gaussian bandpass

2   filter used has a central frequency of 0.048 c/ka and a bandwidth of 0.0070 c/ka.

3   Sedimentation rates at Site U1313, implied by linear interpolation between control

4   points used for timescale construction, are represented in Fig. 3c.

5

6   Figure 4: (a) *Globigerina bulloides* δ^{18}O, (b) *Cibicidoides wuellerstorfi* δ^{18}O and (c)

7   *C. wuellerstorfi* δ^{13}C on the final timescale. The substages nomenclature of MIS 21

8   defined in Ferretti et al. (2010) has been reorganised by using lettered substages

9   (analogous to 5a to 5e in the late Pleistocene) instead of decimal isotopic events.

10

11   Figure 5: The residual obtained by subtracting the Gaussian interpolation from the

12   measured records of (a) *Globigerina bulloides* δ^{18}O, (b) *Cibicidoides wuellerstorfi*

13   δ^{18}O, (c) *C. wuellerstorfi* δ^{13}C. Also shown is the Gaussian interpolation of the three

14   isotopic records using a 15 kyr Gaussian window (black solid line) together with the

15   three measured records (gray solid line) for stratigraphic reference. The wide-

16   Gaussian window (low periodicity) filtered data were linearly interpolated onto the

17   age values of the original data in order to conserve the original variance of the data,

18   and the difference obtained.

19

20   Figure 6: Cross-spectral analyses of the (a) planktonic δ^{18}O residual (blue line) vs. the

21   benthic δ^{18}O residual (red line) and (b) the benthic δ^{18}O residual (red line) vs. the

22   benthic δ^{13}C residual (green line) from IODP Site U1313 using Blackman-Tukey

23   methods. The time series were interpolated at 0.3 kyr intervals by using a Gaussian

24   interpolation with a 1 kyr Gaussian window, linearly detrended, cross-spectra

25   calculated for 150 lags and normalized to unit variance. In each panel, the top section

1 shows the linear power spectrum, the central section displays coherency with the 80%

2 and 95% confidence limits (orange and red horizontal lines) and the bottom shows the

3 phase. Red lines in the phase plots indicate upper and lower error estimates. A

4 negative phase in Fig. 6a implies that the benthic $\delta^{18}O$ leads planktonic $\delta^{18}O$ at a

5 specific coherent band, whereas a positive phase in Fig. 6b indicates that the benthic

6 $\delta^{13}C$ lags benthic $\delta^{18}O$. The bar labelled BW indicates the bandwidth. Brown

7 University ARAND software was used for these analyses.

8

9 Figure 7: Wavelet analysis of the *G. bulloides* $\delta^{18}O$ residual and *C. wuellerstorfi* $\delta^{18}O$

10 residual. For wavelet analysis, the residuals were interpolated at a constant 1 kyr time

11 interval. For reference, the time series together with the precession parameter (Laskar

12 et al., 2004) is shown. Note that spectral power at the suborbital periods in the proxy

13 record is stronger between 880-830 ka when the precession forcing has relatively

14 large amplitude. At around 780 ka, the 'overshoots' associated with the deglaciation

15 generate spectral components at around 20 kyr and 10 kyr, but not the higher

16 frequency components associated with precession maxima. Note that some variance

17 associated with obliquity is still present in the dataset after high-pass filtering.

18

19 Figure 8: Spectral analysis of *Cibicidoides wuellerstorfi* $\delta^{18}O$ (red line) and

20 *Globigerina bulloides* $\delta^{18}O$ (blue line) residuals from IODP Site U1313 in the depth

21 domain. The residuals were obtained by subtracting a Gaussian interpolation with a

22 0.99 m window width from the measured records; in order to conserve the original

23 variance of the data, the Gaussian interpolation was linearly interpolated onto the age

24 values of the original data, and subsequently the difference was obtained. Variance is

25 shown on a linear scale.

1   Arrows at the top of the figure identify prominent peaks in oxygen isotope variance

2   centred at ~0.84 m and 0.52 m. Using an average sedimentation rate at Site U1313 of

3   ~4.3 cm/kyr, this concentration of spectral power corresponds to ~19.5 kyr and ~12

4   kyr respectively, suggesting that the oxygen records are clearly dominated by cycles

5   with periods near precession and half-precession even before orbital tuning.

6

7   Figure 9: Multiproxy records of IODP Site U1313 between 810 and 740 ka. (a) *G.*

8   *bulloides* $\delta^{18}O$ record (blue line) and abundance of the tetraunsaturated C_{37} alkenones

9   ($C_{37:4}$) (magenta line), indicative of high-latitude waters (Naafs et al., 2011). (b)

10   alkenone-based SST (green line) (Naafs et al., 2011). The gray vertical bar designates

11   an increase in the abundance of the ($C_{37:4}$) that coincides with a decrease in SST and

12   heavier *G. bulloides* $\delta^{18}O$ values: all these proxies are consistent with the presence of

13   cold and less saline polar/arctic waters at the core location resulting from iceberg

14   discharges into the northern North Atlantic. The original timescale for the C37:4 and

15   SST records originally published by Naafs et al. (2011) has been revised by applying

16   the age model developed in this study. (c) Carbon isotope records for benthic

17   foraminifera *C. wuellerstorfi* for the interval 810-740 ka. From ~776 ka (marked by

18   the yellow line), increased amplitude oscillations characterise the benthic $\delta^{13}C$ signal,

19   supporting previous findings of a strong link between iceberg discharge, lowered

20   salinity, and weakening of the thermohaline circulation.

21

22   Figure 10: Comparison of foraminiferal $\delta^{18}O$ residual from Site U1313 with the

23   Earth's orbital parameters and insolation records: (a) the orbital eccentricity (blue line)

24   and precession (orange line) (Laskar et al., 2004); (b) insolation at the Equator in

25   Spring (green line) and Autumn (orange line) (Laskar et al., 2004) together with the

1   upper amplitude envelope of the Equinox forcing (violet dashed line), obtained by

2   combining the maxima from either curve, on the assumption that warming responses

3   would be driven by the higher insolation; (c) the 10-kyr Gaussian bandpass filter of

4   the planktonic foraminiferal δ^{18}O residual (blue line) and the 10-kyr Gaussian

5   bandpass filter of the benthic foraminiferal δ^{18}O residual (red line). The Gaussian

6   filter used has a central frequency of 0.10 c/ka and a bandwidth of 0.01 c/ka; (d)

7   Northern Hemisphere summer insolation (65°N, June-July) (blue line) and Southern

8   Hemisphere summer insolation (65°S, December-January) (light blue line) (Laskar et

9   al., 2004) together with the upper amplitude envelope of the Solstice forcing (violet

10   dashed line).

11

12   Figure 11: Pearson Product-Moment cross-correlation at 1 kyr steps for the upper

13   amplitude envelopes of the 10-kyr filtered planktonic and benthic foraminiferal δ^{18}O

14   residual versus the upper amplitude envelopes of the Equinox and Solstice forcings

15   over the entire 1.5 million year interval. The 10 kyr amplitude modulation of the

16   interval of time represented by our data (*c.* 740-910 ka) compared to the amplitude

17   modulation of Equinox and Solstice forcings shows that the time interval where the

18   planktonic data fits the forcing best in the last 1.5 million years, with a r^2 of 0.915, is

19   at 762 ka start age for the equinoctial forcing. The benthic amplitude modulation is

20   similar, with a correlation to the equinoctial forcing of better than 0.849 starting at

21   755 ka. Both the planktonic and benthic response at 10 kyr also make a good fit with

22   the forcing at 380 ka and 0 ka.

23

24   **Table**

25   Table 1: Age model for Site U1313

1   The age control points used to construct the time series in Figure 4. Ages of samples

2   between these control points were estimated by linear interpolation.

1   **Table**

2   Table 1: Age model for Site U1313

3   The age control points used to construct the time series in Figure 4. Ages of samples

4   between these control points were estimated by linear interpolation.

Table 1

Age (ka)	Depth (rmcd) *Naafs et al. (2012)*	Depth (mcd) *Expedition 306 Scientists (2006)*
746	36.47	36.09
772	37.39	37.44
791	38.42	38.41
816	39.72	39.64
832	40.37	40.24
852	41.30	41.06
866	41.70	41.36
912	43.41	43.28

Figure 1
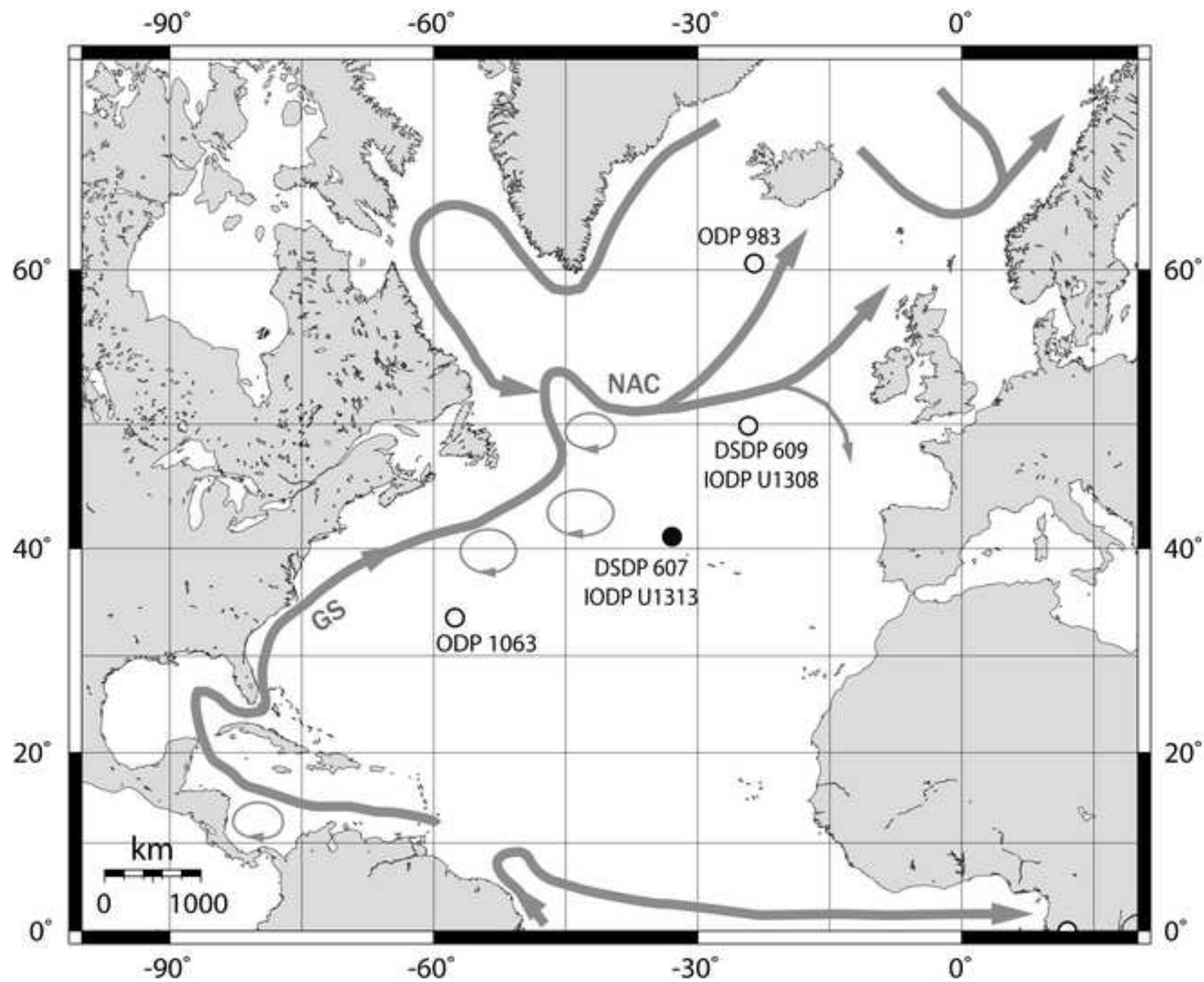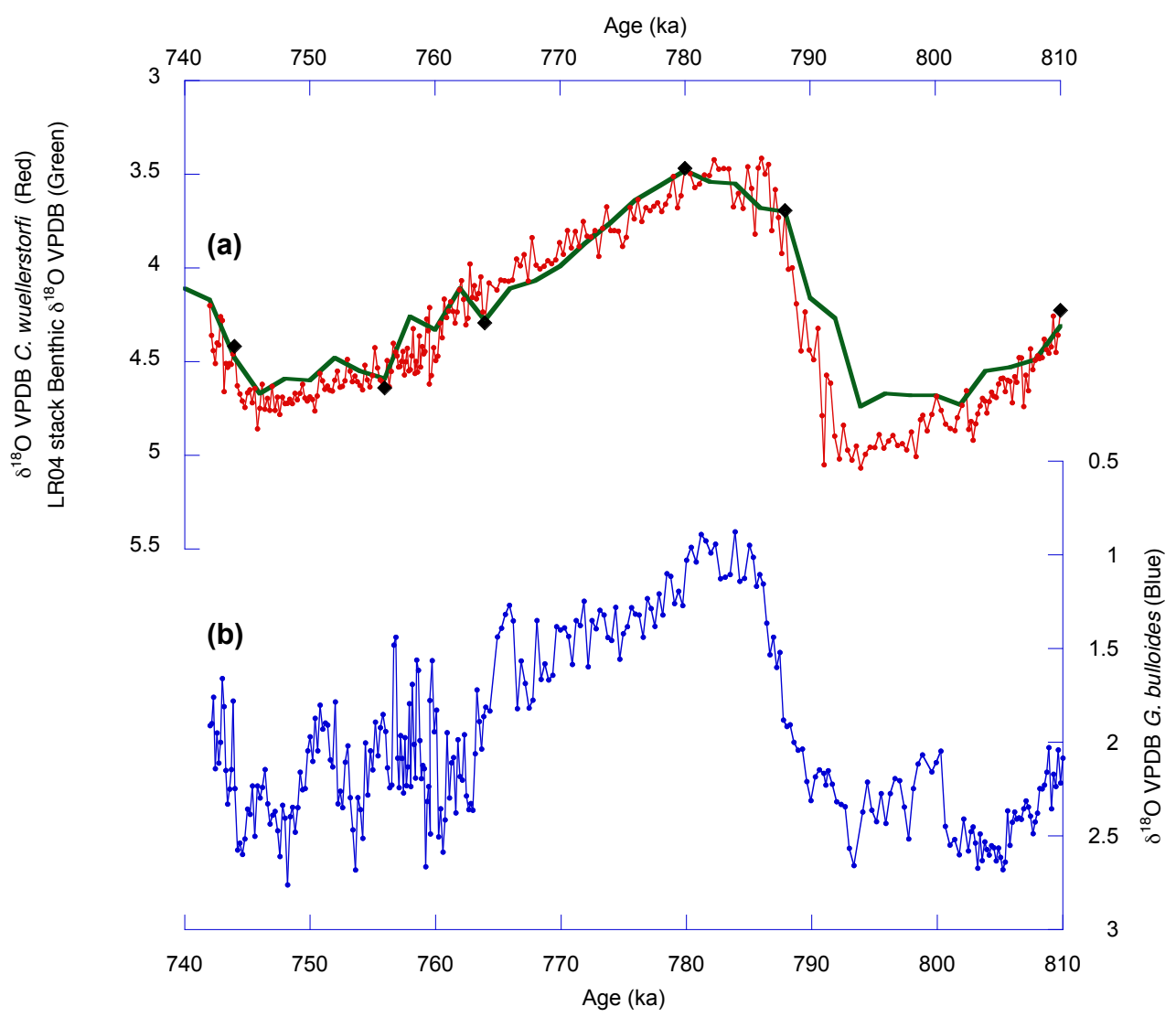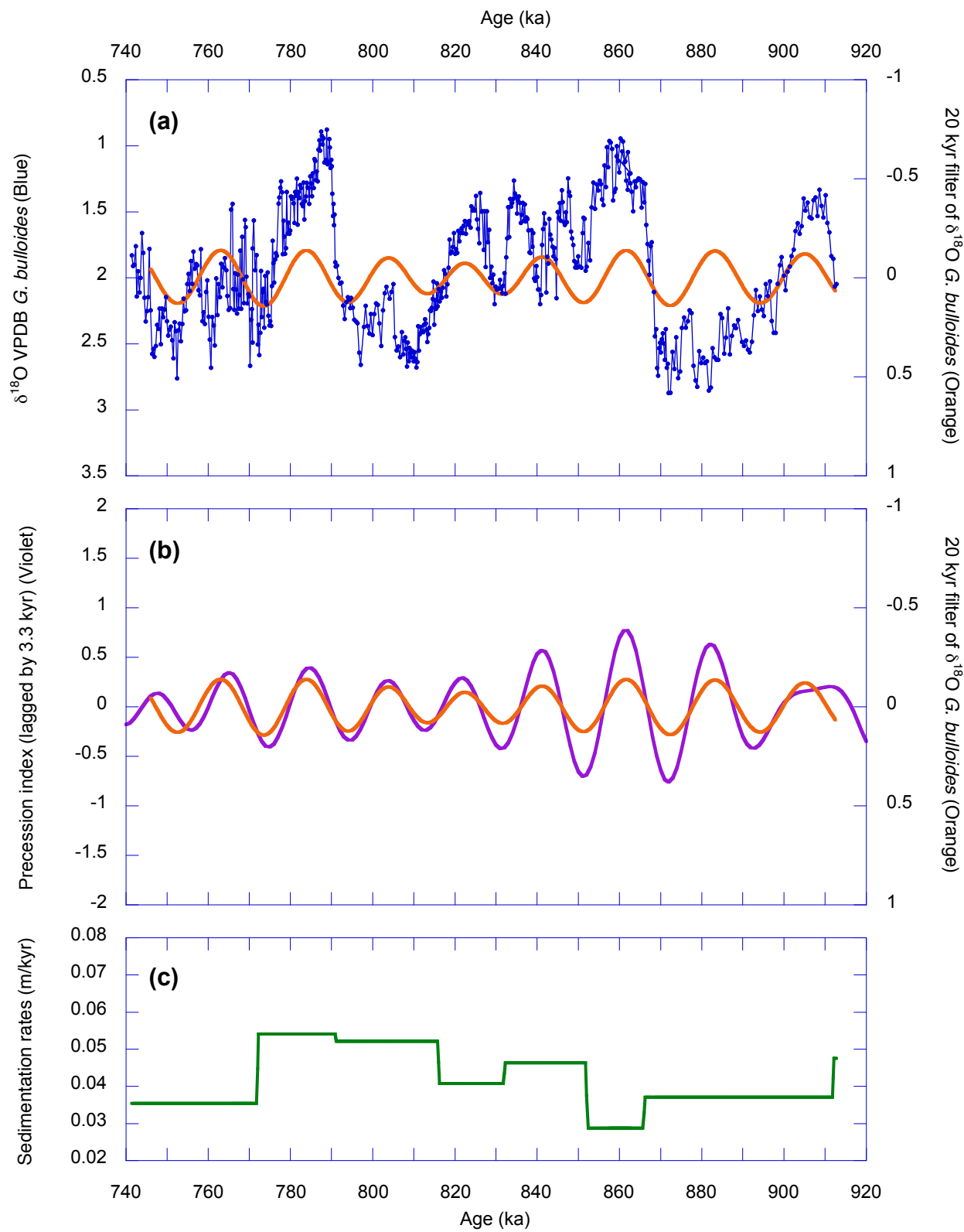
*Figure 2

Figure 3

*Figure 4
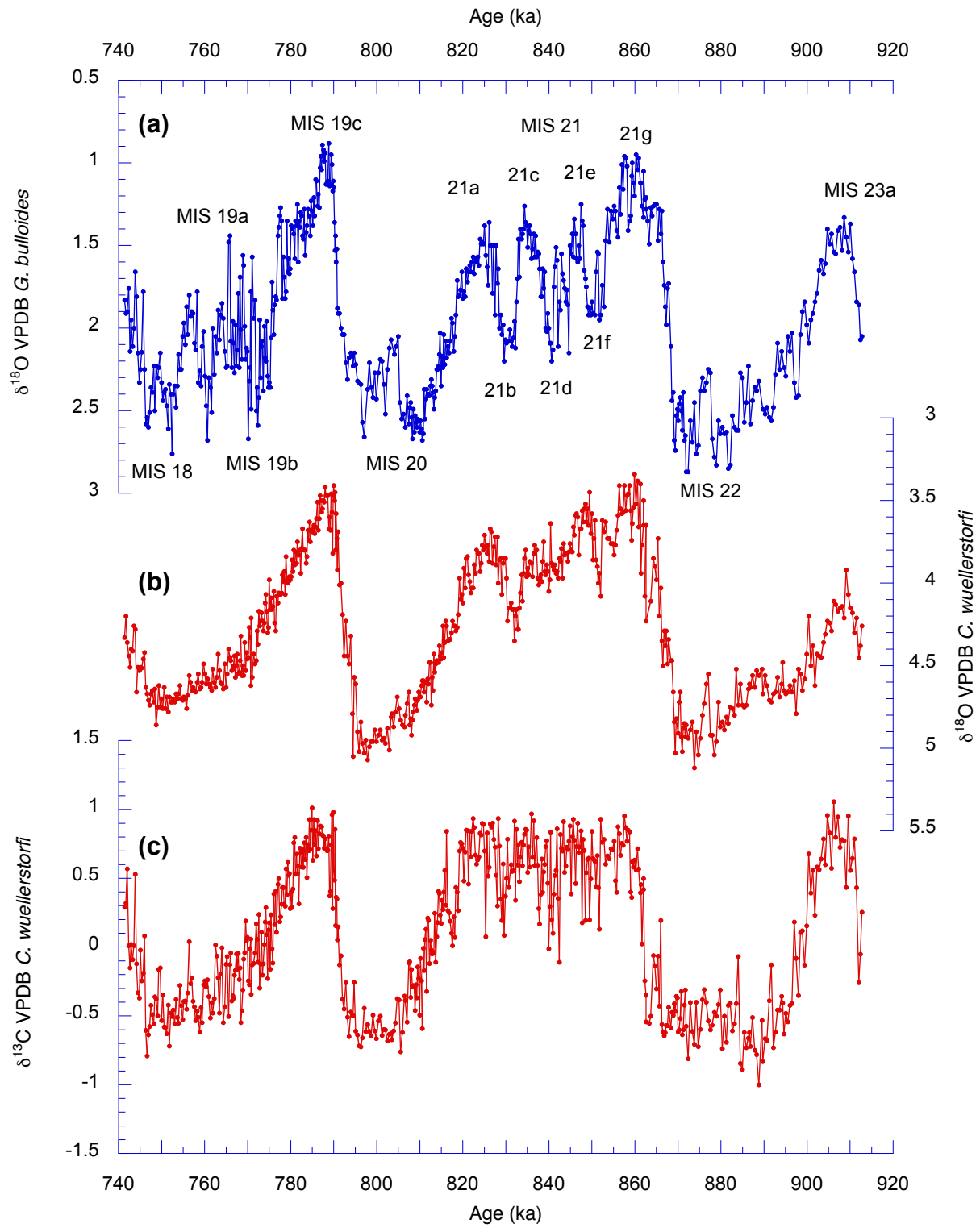
*Figure 5
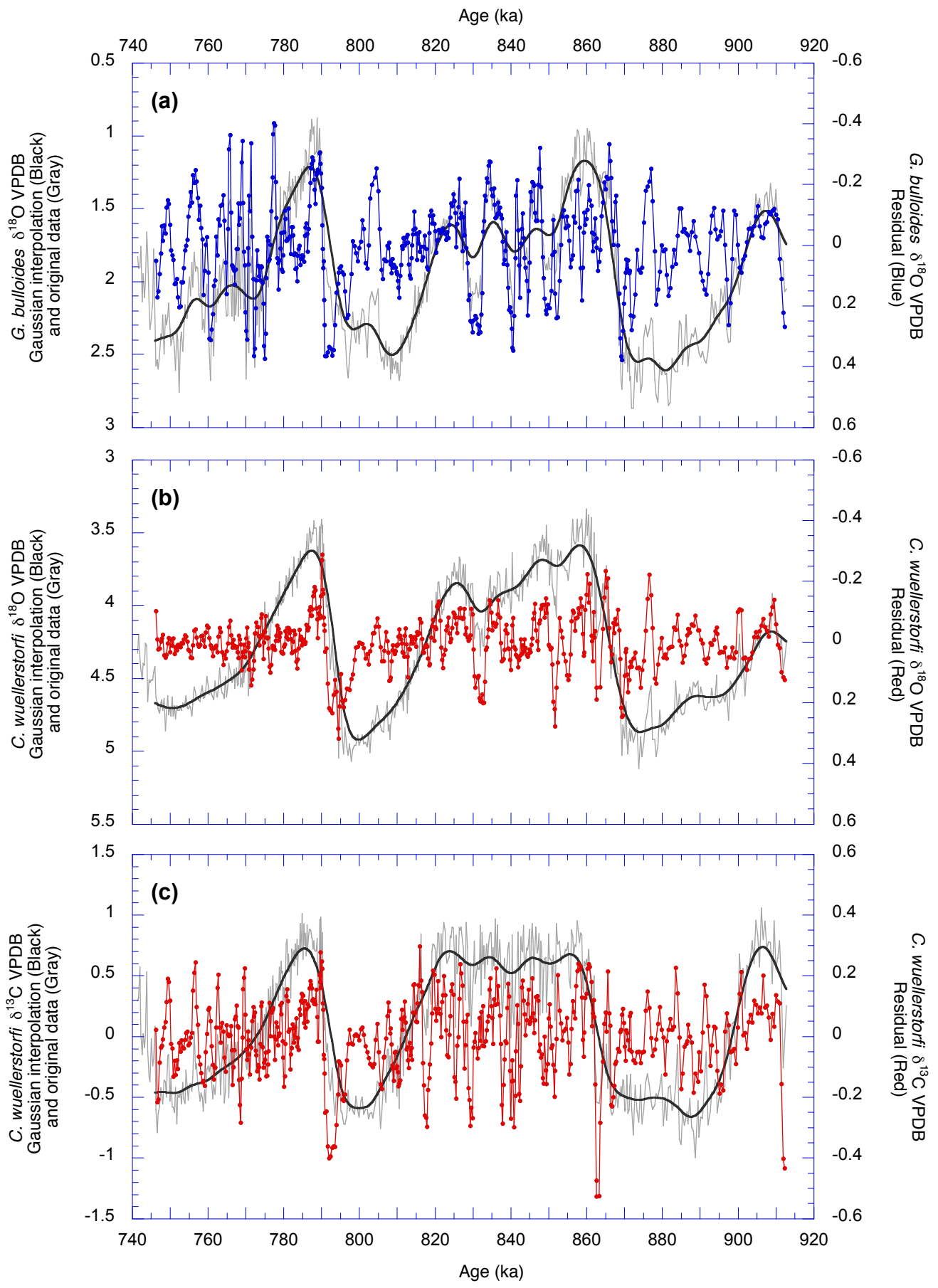
Figure 6a
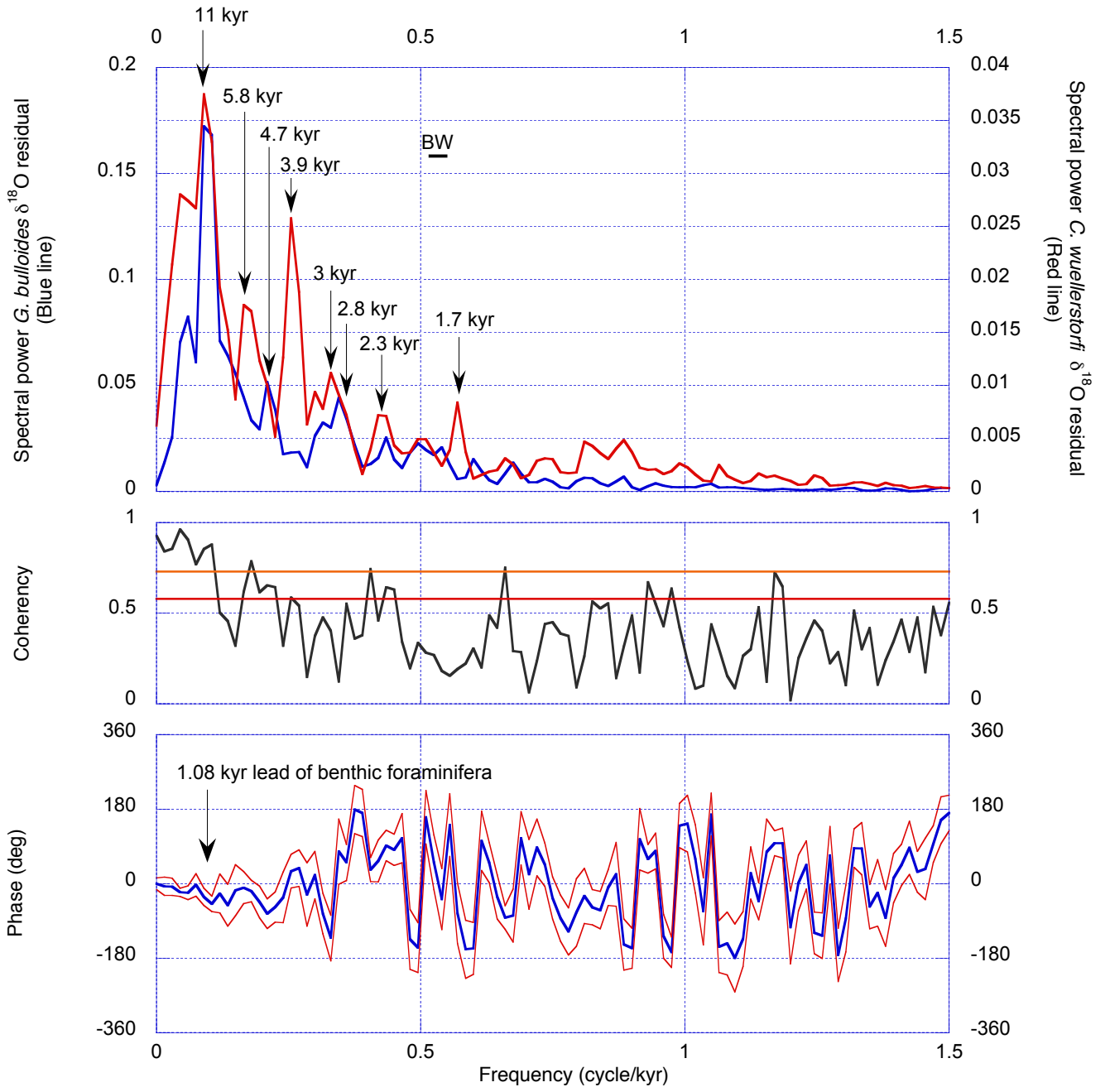
Figure 7
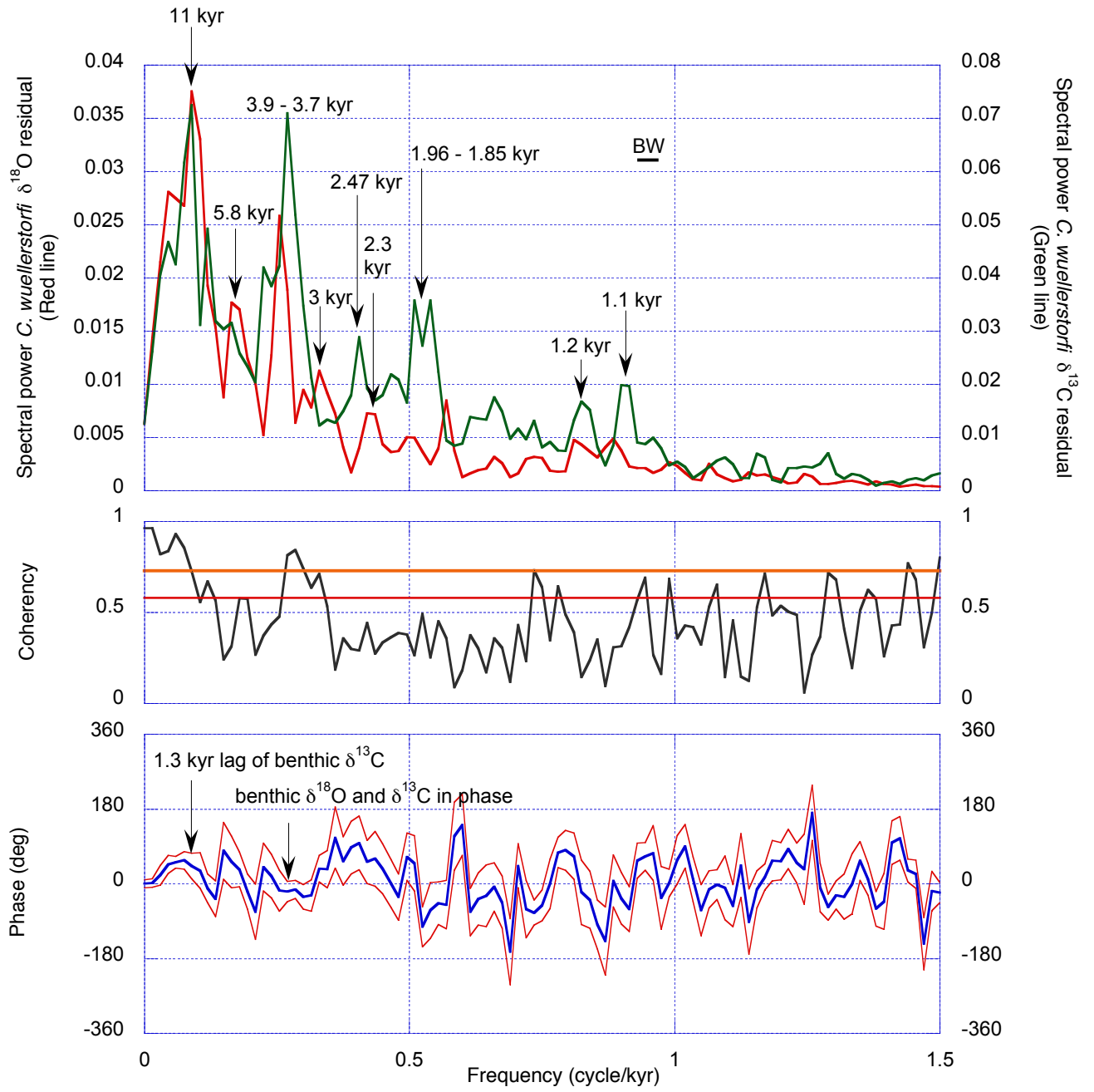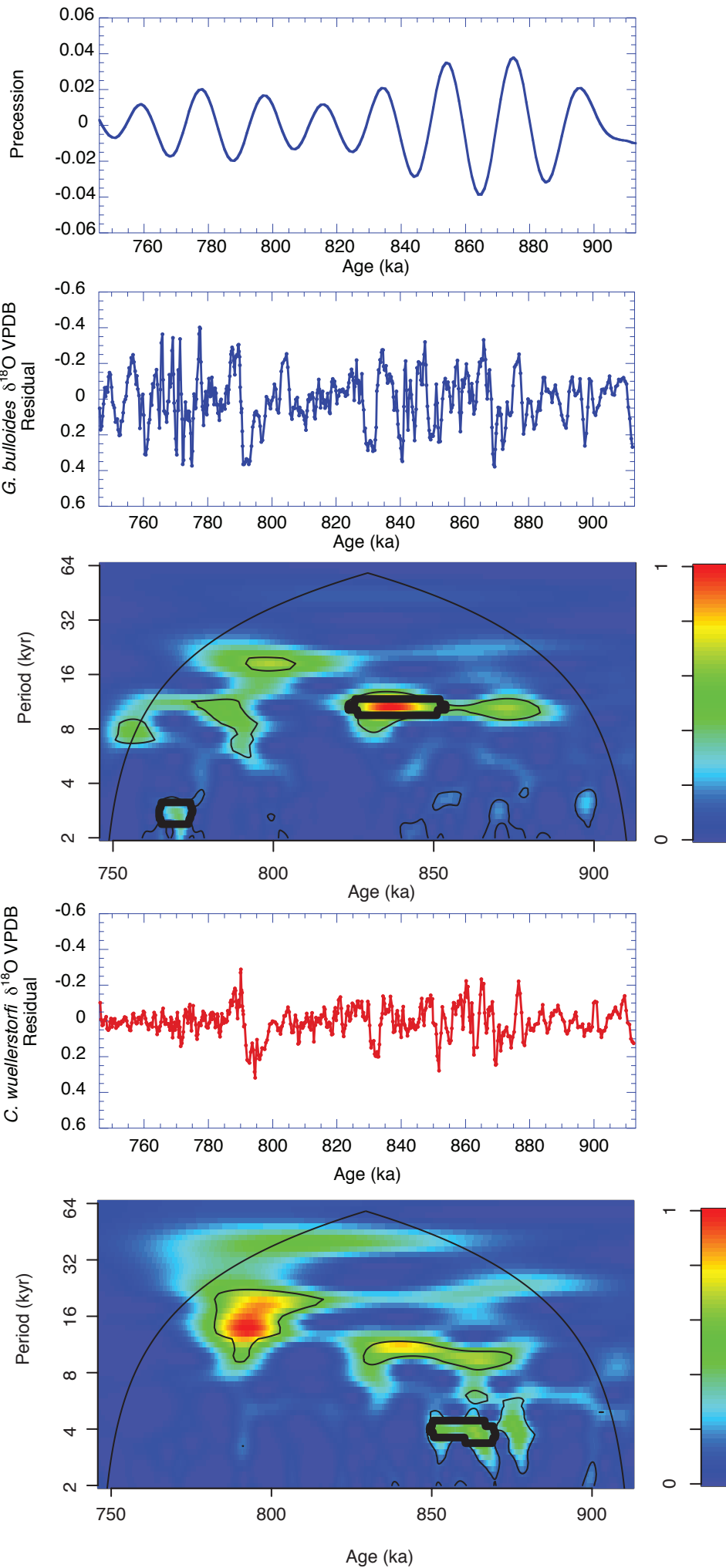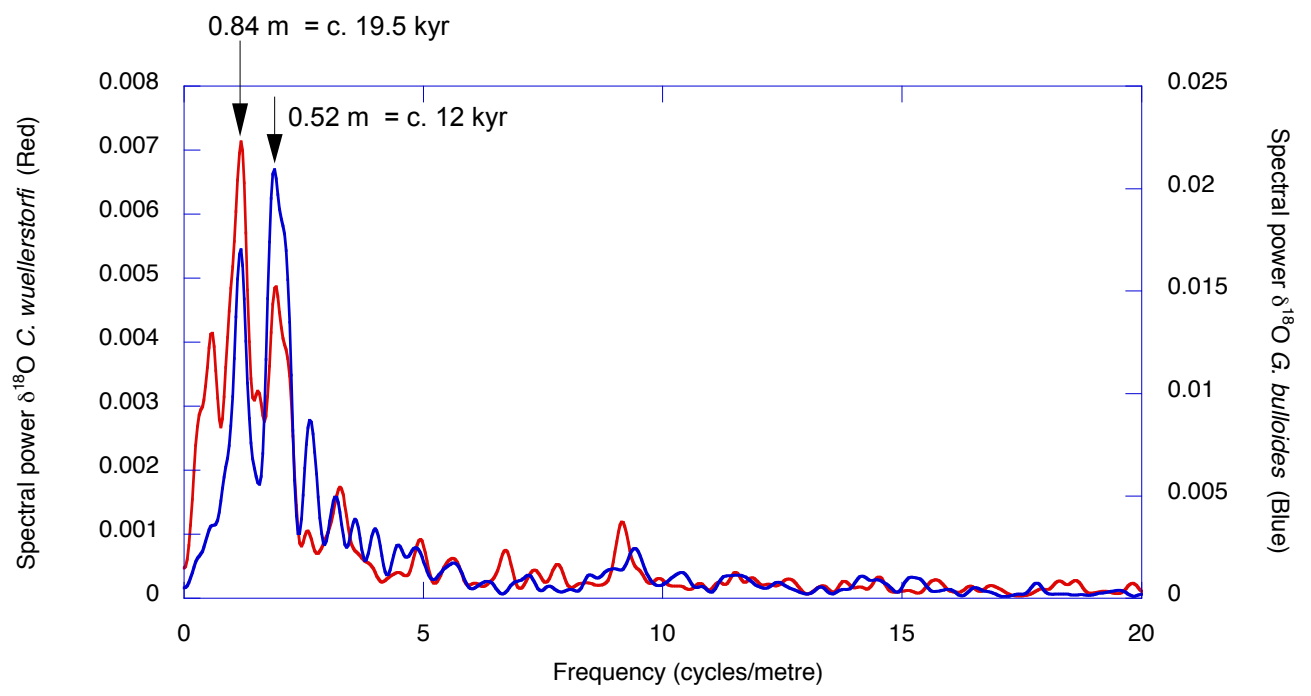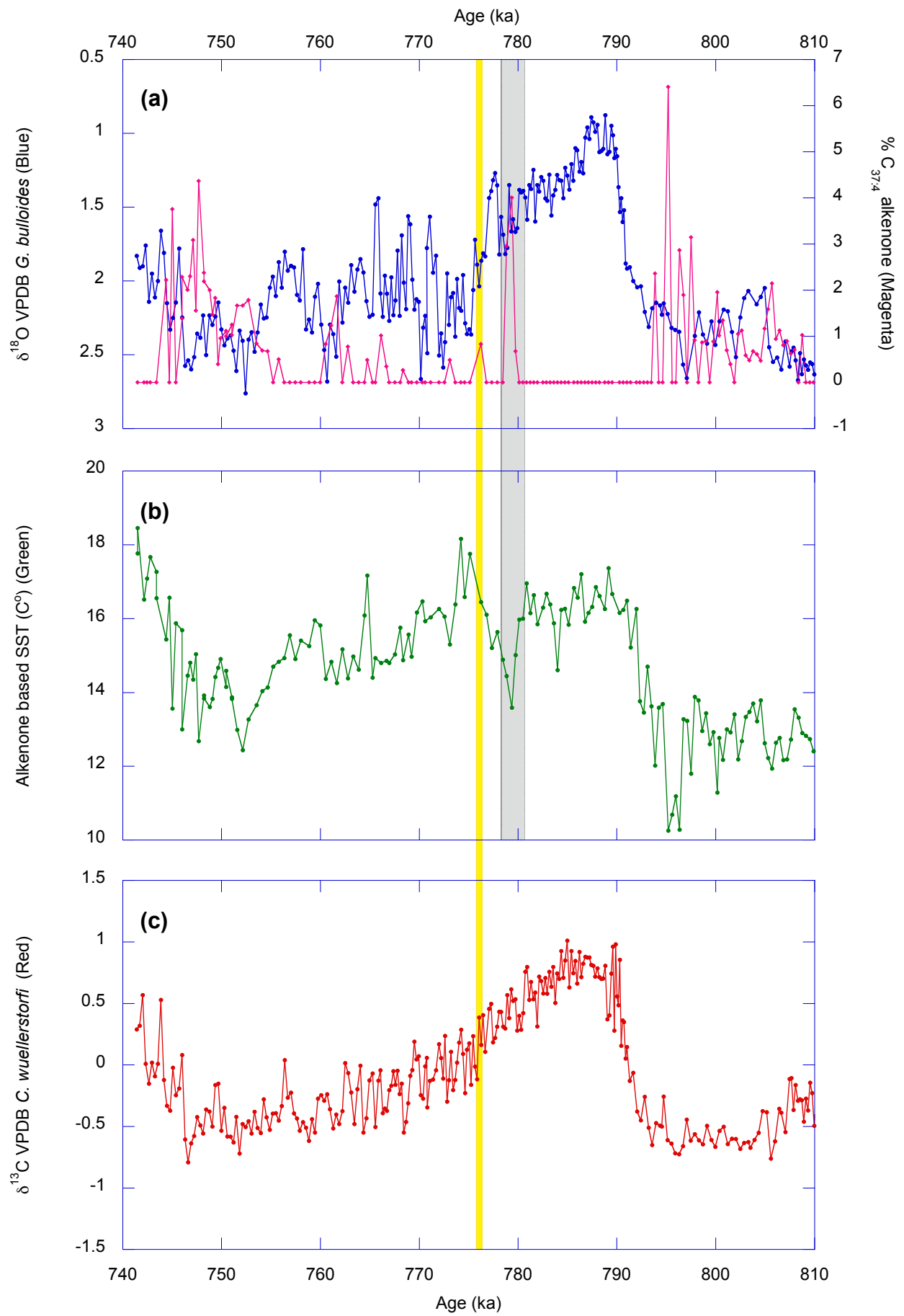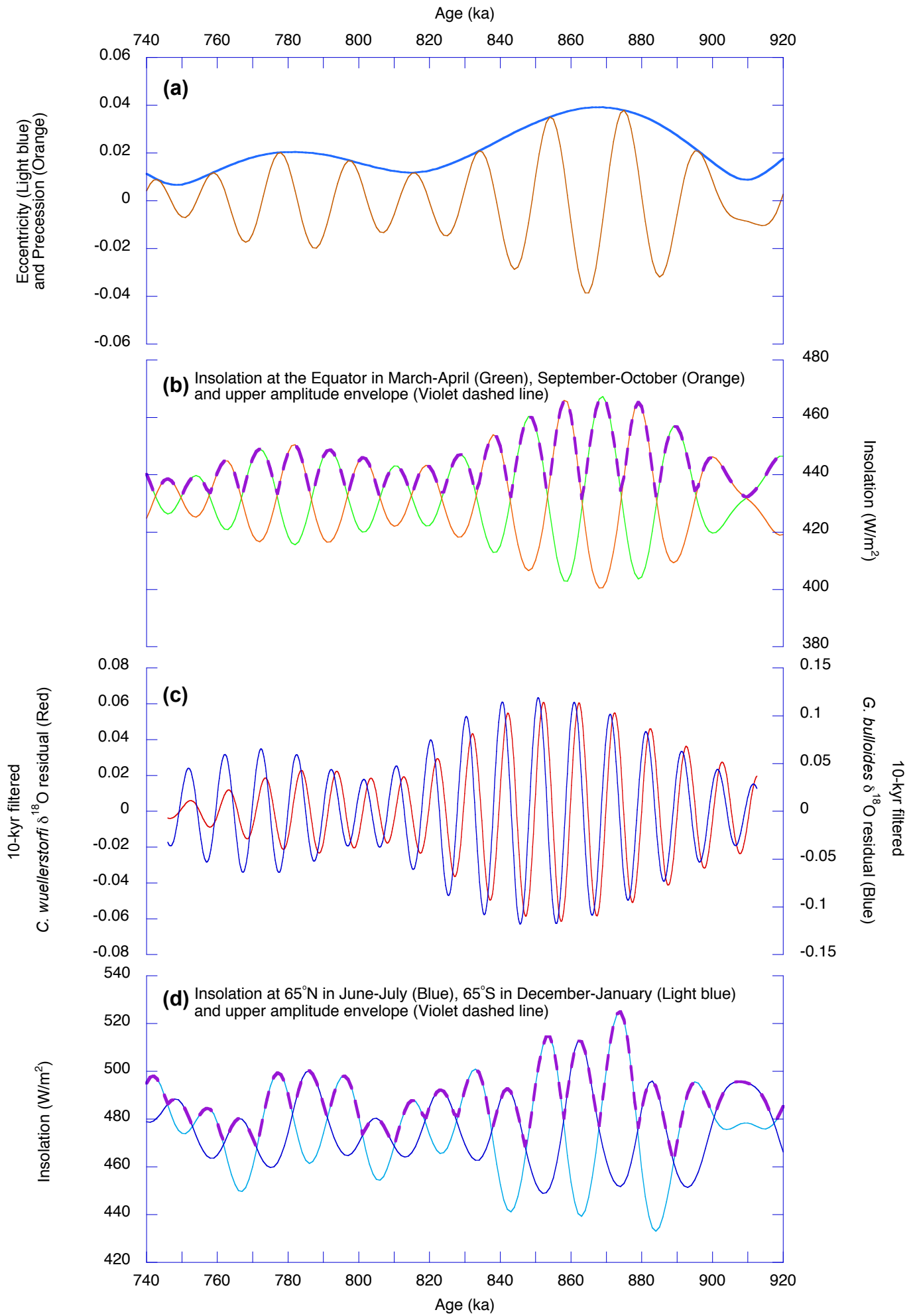
Figure 9

Figure 10

Figure 11
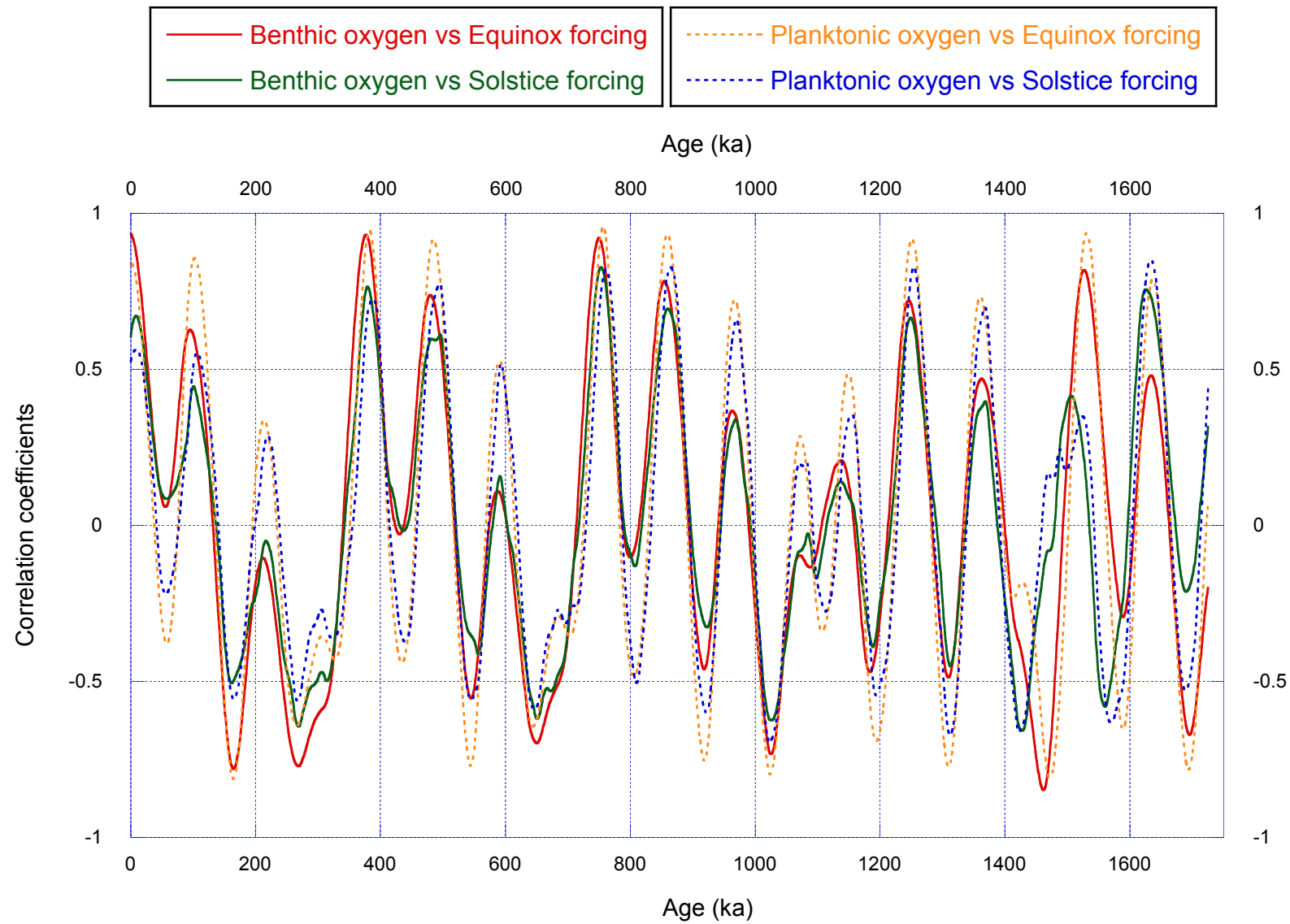
Supplementary Text

Supplementary Figure S1
Click here to download Supplementary Data: FigureS1.pdf

Supplementary Figure S2

Supplementary Figure S3

Supplementary Figure S4

Click here to download Supplementary Data: FigureS4.pdf

Supplementary Figure S5